UNIVERSITETET
I OSLO

Thesis for the degree: Master of science – December 2022

Histidine methylation of ZnT family zinc transporters by the methyltransferase METTL9

Investigation into potential METTL9-mediated histidine methylation of ZnT5 and ZnT7

Anniken Johnsen

Molecular Biology and Biochemistry
60 credits

Department of Biosciences
Faculty of Mathematics and Natural Science

Summary

Post-translational modifications (PTMs) provide an additional layer of functionality to the proteome of various organisms. Out of the most common forms of PTMs, methylation, which involves the transfer of a -CH_3 group from a donor to a substrate, is one of the smallest but can still have large effects. In biological systems the most commonly used donor is S-adenosyl-L-methionine (SAM), and the methylation is mediated by enzymes known as methyltransferases (MTases).

Methylation of the side chains of two amino acids in particular, namely lysine and arginine, are now recognized as textbook examples of protein regulation. Methylation of other amino acids, such as histidine, is not as well characterized. For histidine, this is largely due to the fact that protein histidine MTases or PHMTs, have remained largely elusive until recently. Histidine can be mono-methylated at one of two nitrogen atoms (N1 and N3) found in the imidazole ring of its side chain yielding 1-methylhistidine (1MH) or 3-methylhistidine (3MH) respectively. Since 2018, three human PHMTs, have been characterized, these are SETD3, METTL9 and METTL18. SETD3 and METTL18 both yield 3MH, whereas METTL9 has been shown to generate 1MH modifications in proteins.

METTL9 was characterized by our group in 2021 as the first known 1MH-specific PHMT, and it was elucidated that METTL9 recognizes a specific motif of alternating histidine residues separated by a small, uncharged amino acid (HxH-motif). A particular class of proteins, the transmembrane zinc transporters, have histidine-rich regions in their loops and near their N-terminus, which are dense in alternating histidine residues making these proteins a very interesting subset of potential METTL9 substrates. To date, only one such zinc transporter, ZIP7, has been identified as an *in vivo* substrate of METTL9.

This thesis focuses on the investigation of two zinc transporters, ZnT5 and ZnT7, as potential METTL9 substrates. GFP-tagged proteins were overexpressed in wild type (WT) and METTL9 knock out (KO) cells, and subcellular localization was investigated via microscopy, with localization being consistent of the early secretory pathway as has been reported in the past. Full-length ZnT7 was identified as an *in vitro* substrate of METTL9 via fluorography, and when 1MH content of GFP-tagged ZnT7 was analyzed by amino acid analysis (AAA) there was a significant increase observed in the WT cells compared to METTL9 KO cells. Together these results indicate that the zinc transporter ZnT7 is an *in vivo* substrate of METTL9, and methods used during the work performed in this thesis can be applied to other zinc transporter proteins in the future, to investigate them as substrates of METTL9.

Acknowledgments

The work presented in this thesis was carried out in the laboratory of Professor Pål Ø. Falnes at the Department of Bioscience, The Faculty of Mathematics and Natural Science, University of Oslo.

I would like to humbly thank Professor Pål Ø. Falnes for giving me the opportunity to be a part of this project, as well as for answering questions (and emails) at all hours of the day. To my lab-supervisor, Erna Davydova, I would like to express my deepest gratitude, without you this thesis would have never been completed. For making what might be considered repetitive lab work a delight, I am eternally grateful. Your continued tips and comments during the writing of this thesis have been highly appreciated and valued.

I would also like to thank my co-lab supervisor, Lisa Schroer, for being incredibly helpful with both lab-work and writing and for providing a great deal of laughs on long, stressful days.

To Shabitha Amarasingham: I would have never survived these past two years without you, and our laughs shared together in the lab will be deeply missed. Thank you for always brightening up my day.

I would also like thank all current and former members of the Falnes group for always being helpful and kind throughout these past two years. For insightful feedback during presentations and insightful discussions during lab-meetings, I am also very grateful.

I would also like to thank both family and friends for being incredibly supportive and constantly providing me with encouraging words all throughout my degree. To my boyfriend Jakob, thank you for your patience and for always being there for me.

Abbreviations

% - Percent
α - Alpha
β - Beta
µ - Micro
^{3}H - Tritium
7BS - Seven- β-strand
°C - Degree Celsius

AAH - Amino acid hydrolysis
AAA - Amino acid analysis
BSA - Bovine Serum Albumin
Ci/mmol - Curies per millimole
DMEM - Dulbecco's Modified Eagle's Medium
DNA - Deoxyribonucleic acid
dNTPs - Deoxynucleotide
E.coli - *Escherichia coli*
EDTA - Ethylenediaminetetraacetic acid
FBS - Fetal Bovine Serum
GFP - Green fluorescent protein
GST - Glutathione-S-transferase
HCl - Hydrochloric acid
hsMETTL9 - *Homo sapiens* METTL9
IMDM - Iscove's Modified Dulbecco's Medium
IP - Immunoprecipitation
JmjC - Jumonji C
KDM - Lysine demethylase
KO - Knock out
LB - Luria Broth
M - Molar
MES - 2-(N-morpholino)ethanesulfonic acid
METTL9 - Methyltransferase-like protein 9
min - minutes
MS - Mass spectrometry
MTase - Methyltransferase
mqH_2O - Milli-Q purified water
n - nano
NaCl - Sodium chloride
nt - nucleotide
PAGE - Polyacrylamide Gel Electrophoresis
PBS - Phosphate buffered saline
PCR - Polymerase chain reaction
PHMT - Protein histidine methyltransferase
PKMT - Protein lysine methyltransferase
PRMT - Protein arginine methyltransferase
P/S - Penicillin Streptomycin
PTM - Post-translational modification

RNA - Ribonucleic acid
RT - Room temperature
s - seconds
SAH - S-adenosyl-L-homocysteine
SAM - S-adenosyl-L-methionine
SDS - Sodium dodecyl sulfate
SET - Su(var)3-9, Enhancer-of-zeste, Trithorax
TAE - Tris-acetate EDTA
TBS - Tris-buffered saline
TBS-T - Tris-buffered saline with 0.1% Tween
V - Volt
WT - Wild type

Table of contents

1. Introduction

1.1 Post-translational modifications and the diversity of the human proteome

Proteins are large biomolecules which play a critical role in many biological processes including the structure, function, and regulation of cells and tissues in various organisms [1].
The function of a protein is primarily defined by the sequence of amino acids which is encoded by the DNA sequence of the gene. In addition, the function of a protein can also be affected by post-translational modifications (PTMs), which contribute to making the human proteome more diverse than the actual protein sequence encoded by the genome [2]. PTMs are chemical modifications that regulate protein activity, localization, interactions and folding [3]. Thus, PTMs add an additional layer of functional diversity to cellular proteins.

PTMs occur on distinct amino acid side chains, and they are most often mediated by enzymatic activity. PTMs can occur after mRNA translation at several stages during the “life” of a protein. PTMs occurring after translation and prior to folding can assist with both protein folding and protein stability [4]. PTMs occurring at this stage can also play roles in directing the protein to its proper cellular localization [4, 5]. PTMs occurring after folding and localization, are in most cases related to maintaining proper protein activity, and assist in activation or inactivation of said activity [4]. In eukaryotes the most studied forms of PTMs include phosphorylation, acetylation, glycosylation, ubiquitination, succinylation, sumoylation and methylation [5].

1.2 SAM-dependent methylation

One of the most common forms of PTMs on protein or peptide sequences is methylation. Methylation reactions are reactions where methyltransferase enzymes (MTases) mediate the transfer of a methyl group (CH_3) from a donor to a substrate such as DNA, RNA, or protein [6]. In both prokaryotes and eukaryotes, the major methyl donor is S-adenosyl-L-methionine (SAM; also referred to as AdoMet in literature, Figure 1) [6]. The methyl group of SAM is bound to the molecule through a positively charged sulfur atom making what is known as a methyl thiol [6]. This methyl thiol moiety is very reactive towards polarized nucleophiles such as nitrogen (N), oxygen (O), and sulfur (S) as well as activated carbon (C) atoms [6]. This is exploited by SAM-dependent MTases which bring SAM into contact with the nucleophilic groups of substrates [7] and deprotonate the substrate, freeing up an electron pair so that it can make a nucleophilic attack on the methyl group of SAM, as illustrated in Figure 1.

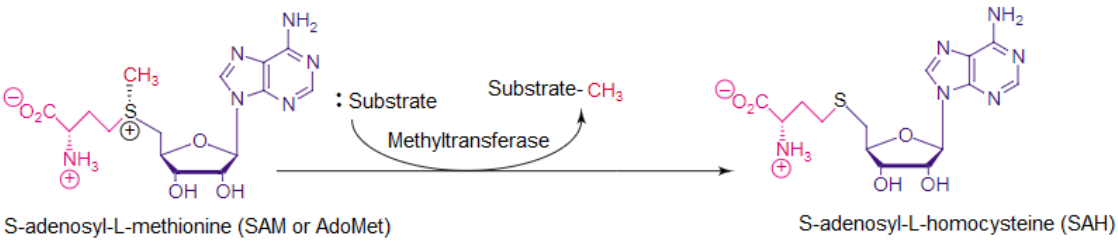

Figure 1: Generalized schematics of the methylation reaction mediated by SAM-dependent MTases. The central sulfur atom is shown in black, and the methyl group being transferred is shown in red. Figure is adapted from [7].

1.3 SAM-dependent methyltransferases

A substantial percentage of proteins across all organisms are enzymes capable of transferring a methyl group from SAM to a distinct substrate, namely MTases. In the human genome alone, there are encoded more than 200 predicted MTases [8]. Most MTases vary in their overall 3D structure, but within the active site their properties remain conserved [9]. MTases are found in a small number of distinct structural arrangements which, along with partly conserved amino acid sequences, are used to group them into classes [8, 10]. An overview of these classes is shown in Figure 2.

The largest class of MTases is the seven-β-strand (7BS) family, which contains enzymes responsible for methylating a wide range of substrates, including DNA, RNA and proteins [11]. The second largest class is the so-called SET (Su(Var)3-9, Enhancer-of-zeste, Trithorax) domain proteins [12]. All characterized SET-domain MTases are known to only methylate lysines [12] with the exception of SETD3, which is a histidine-specific MTase, recently shown to methylate histidine in actin [13]. In addition, there are other smaller families of MTases, not all of which are dependent on SAM [8, 14].

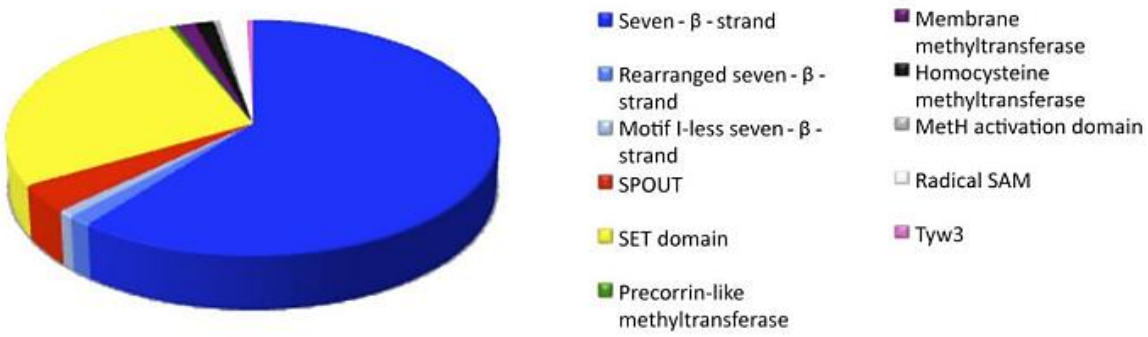

Figure 2: Overview of human methyltransferase classes. Fractional composition of the predicted and characterized MTases in the human methyltransferasome, showing that the 7BS MTases is by far the largest class, followed by the SET-domain proteins. Figure is adapted from [8].

1.4 Protein methylation

Methylation of proteins by SAM-dependent MTases occurs on either an oxygen (O), nitrogen (N), carbon (C) or sulfur (S) atom, in the side-chain of the acceptor amino acid or at the N- or C-termini of the protein [6, 15]. Protein methylation mainly occurs on the side chains of lysine (K) and arginine (R), but other amino acids such as histidine can also be methylated [16].

Lysine and arginine are both basic amino acids capable of being methylated on nitrogen residues of their side chains. The side chain of lysine contains a terminal ε-amino group capable of accepting up to three methyl-groups, yielding mono-, di- or tri-methylated lysine [17], as can be seen in Figure 3. SAM-dependent MTases responsible for methylating lysine in proteins are known as protein lysine MTases or PKMTs, most of which belongs either to the SET-domain protein family or to the 7BS family of MTases [11, 16]. The side chain of arginine contains two nitrogen atoms, one or both of which can be methylated yielding either mono- or di-methylarginine, the latter of which there are two forms of: symmetric or asymmetric [16], as can be seen in Figure 3. MTases mediating the methylation of arginine residues are known as protein arginine MTases or PRMTs, all of which belong to the 7BS family of MTases [16].

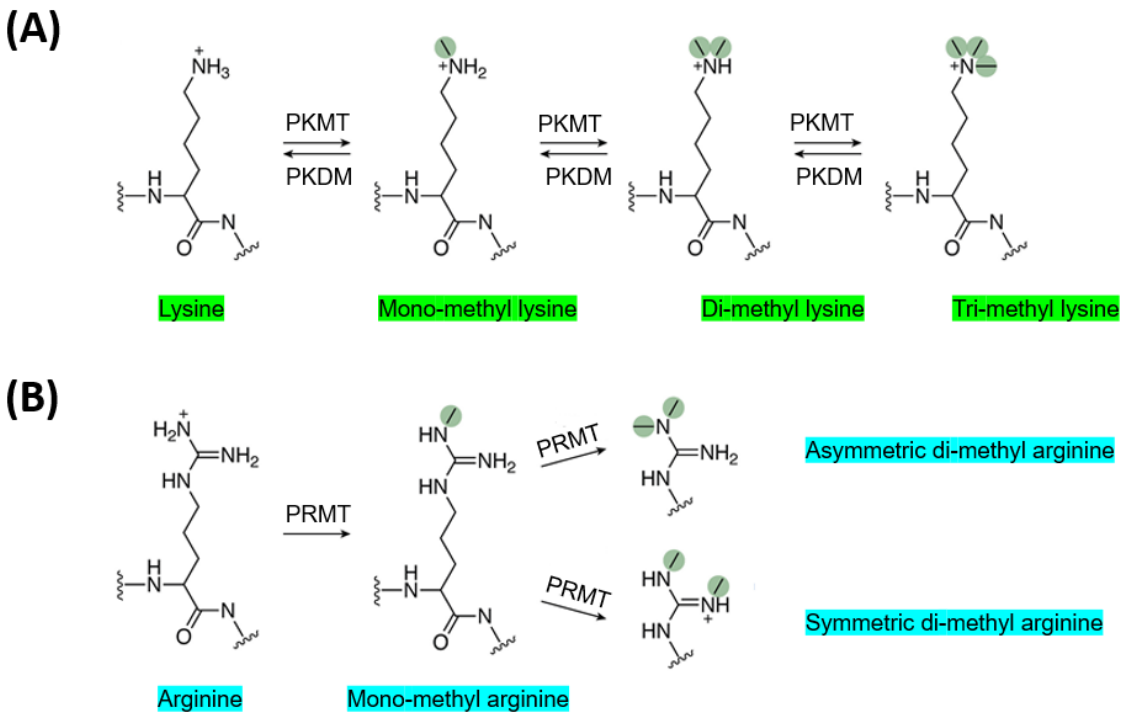

Figure 3: Methylated states of (A) lysine and (B) arginine (B). (A) Protein lysine MTases (PKMTs) can introduce up to three methyl-groups yielding mono-, di- or tri-methylated lysine. (B) Protein arginine MTases (PRMTs) can yield mono-, or di-methylated arginine, where the latter can exist in an asymmetric or symmetric form. Figure adapted from [18].

Protein lysine and arginine methylation is particularly abundant on the flexible tails of histone proteins, where the methylation of specific lysine or arginine residues serves as “marks”, typically to either activate or repress transcription [19]. Marks are recognized by various proteins which often contain reader-domains recognizing specific methylation marks [16]. Once these marks have served their function, they can be removed by various demethylase enzymes. Lysine demethylases (KDMs) serve as “erasers” of lysine methylation. To date, two families of KDMs, known as the LSD family or amine oxidases [20, 21] and the JmjC demethylases [22] have been characterized. Demethylation of arginine residues is not as well characterized though there is some evidence pointing towards certain KDMs also being capable of demethylating arginine [23]. In addition, one protein known as Jmjd6 was shown by one study to have arginine demethylation activity [24], however, it is still debated whether true arginine demethylases exist.

As methylation of histone proteins regulates the chromatin structure and participates in epigenetic regulation of gene expression in numerous biological processes including development and differentiation [25], research into this field has been immense. However, methylation also occurs on non-histone proteins [26], where the modification has been shown to control protein activity and in addition serves key roles in the regulation of stability, enzymatic activity, subcellular distribution, and interaction with other proteins [27]. In addition, methylation

of non-histone proteins can also affect other cellular functions such as signaling, DNA repair and gene transcription [17, 28, 29]. To additionally demonstrate the importance of methylation, it has also been shown that if this regulation system is disrupted human diseases such as cancer can arise [17, 30].

1.4.1 Histidine methylation

The methylation of lysine and arginine residues has been heavily researched and are frequently used as textbook examples of protein regulation. In comparison, methylation of other amino acids, and the purpose of the methylation has gained less attention. One such amino acid is histidine, whose presence in both actin [31, 32] and myosin [33] was observed in the late 1960s to early 70s. Regardless, histidine methylation remains a rather elusive PTM, predominantly because identification of the enzymes responsible for introducing this modification has been lacking, until recently.

Histidine has a side chain made up of an aromatic imidazole ring containing a proximal nitrogen, N1 (or π) and a distal nitrogen, N3 (or τ). Either or both of these nitrogen atoms can be protonated [34], which at physiological pH, allows histidine to exist in either a neutral or a positively charged state [34]. In the neutral state, when only one nitrogen atom is protonated, the proton can switch between the two nitrogen atoms in a process known as tautomerization [34]. The basic nitrogen in histidine can act as a coordinate ligand for metal cations such as zinc [34, 35].

Histidine can be mono-methylated on these nitrogen atoms by enzymes known as protein histidine MTases, or PHMTs. Methylation of N1 yields 1-methylhistidine (1MH) and methylation of N3 yields 3-methylhistidine (3MH) [18], as can be seen in Figure 4. The methylated forms of histidine are not interchangeable, meaning the potential for tautomerization is lost upon methylation [18].

In a 2021 proteomics study by Kapell and Jakobsson [36], it was demonstrated that histidine methylation is widespread in human cells and tissues. They also observed that histidine methylation is both prominent and present in all major cellular compartments [36], with an overrepresentation in specific protein families, in particular in actin and zinc-binding proteins [36]. This would indicate that histidine methylation has functional significance, and that it is important to investigate this further.

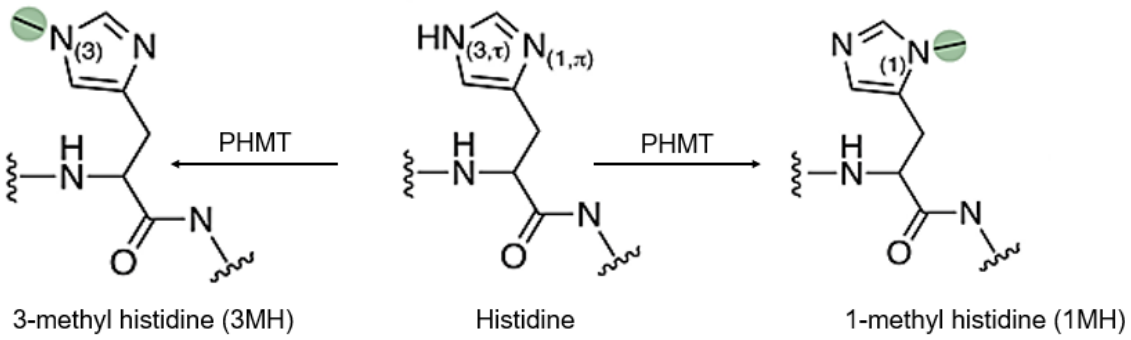

Figure 4: Histidine methylation states. Mechanism of histidine methylation by protein histidine MTases (PHMTs) leading to the production of 3MH (left) and 1MH (right). Figure adapted from [18].

In 2018, more than five decades after histidine was first identified as being methylated in actin proteins [31, 32], the human MTase known as SETD3 was uncovered as the enzyme responsible for this specific modification, namely the 3MH modification of histidine residue 73 in actin proteins [31, 32, 37, 38]. As the name suggests, SETD3 belongs to the SET-domain family of MTases, which prior to its characterization, was thought to be a lysine-specific family [12].

The characterization of SETD3 as the first human PHMT was independently done by two research groups [37, 38]. Wilkinson et.al [38] demonstrated that the 3MH modification in actin regulates actin and is related to muscle contractions. Via a proteomics analysis it was also shown that the 3MH modification of actin is likely the only physiological substrate of SETD3 [38].

In 2010, the ribosomal protein Rpl3 was shown to contain 3MH modifications in budding yeast by Webb et.al [39]. It was further demonstrated that this activity was dependent on an MTase which they named histidine protein methyltransferase 1 or Hpm1. In a study from 2013 [40], the human ribosomal protein RPL3 was reported as a interactant of the human MTase METTL18, which suggested that RPL3 might be a target of METTL18. The enzymatic activity of METTL18 remained elusive until 2021 when Małecki et.al [13] characterized METTL18 as the second human PHMT, mediating 3MH modifications in human RPL3 [13]. By knocking out METTL18 in human HAP1 cells it was shown that these cells displayed an altered pre-rRNA processing as well as decreased polyribosome formation [13]. METTL18 KO cells also showed codon-specific changes in mRNA translation [13], and the authors therefore theorize that methylation of RPL3 might regulate protein synthesis through mRNA translation. In the plasma from patients with colorectal cancer, METTL18 has been reported as being elevated [41], which might suggest that the protein can serve as a cancer biomarker in the future.

In 2021, the first 1MH-specific protein MTase METTL9 was characterized by Davydova et.al [42] using a variety of biochemical and cellular assays. Via an amino acid analysis (AAA) of total protein hydrolysates, they showed that 1MH is a relatively abundant modification and that METTL9 introduced the majority of 1MH in both human and mouse proteomes [42]. This makes METTL9 the only characterized PHMT capable of introducing 1MH in proteins to date, and these findings were subsequently independently validated by a two different groups later that same year [43, 44]. Like METTL18, METTL9 also belongs to the 7BS class of MTases, but with little homology to other enzymes belonging to this class [42]. To date there are few studies on the physiological importance of METTL9 and the 1MH modifications this enzyme mediates, as well as how this relates to disease. Independent genetic studies have linked chromosomal deletion of a segment including METTL9, as well as other genes, to colonic hypoganglionosis [45] and hearing loss [46] and when METTL9 was deleted in human HAP1 cells, the cells displayed abnormalities in both nucleic acid metabolism as well as vesicle-mediated processes [36].

As the three identified PHMTs belong to two different MTase families, this indicates that the ability to methylate histidine has arisen on several occasions during evolution and, as demonstrated by SET-domain in SETD3 and the 7BS-fold in METTL9 and METTL18, that this PHMT activity can develop on different protein folds [18].

1.5 METTL9

METTL9 was predicted to be an MTase already in 2011 by Petrossian and Clarke as one of the more than 200 MTases encoded by the human genome [8], but its function remained unclear until its characterization in 2021 [42-44].

METTL9 belongs to the 7BS class of MTases, but with very little homology to other 7BS MTases, apart from the typical 7BS fold [8], though structure has thus far only been predicted and not solved. METTL9 is, however, highly conserved across all the major supergroups of eukaryotes, with predicted METTL9 orthologs being widespread throughout eukaryote genomes, including animals and many distantly related protozoans, but absent from the genomes of land plants and fungi [42].

The METTL9 enzyme is localized in the ER and the mitochondria [42] and can methylate histidine in a wide variety of substrates [42], which sets METTL9 apart from the two other identified PHMTs, SETD3 and METTL18, who each only have one identified substrate to date.

In the study by Davydova et.al, 2021 [42] METTL9 was shown to catalyze the generation of 1MH in sequences containing alternating histidine residues corresponding to His-x-His (or

HxH) where “x” represents a small, uncharged residue such as alanine (A), asparagine (N), glycine (G), serine (S) or threonine (T). The prevalence of this HxH-motif in previously published proteins containing methylated histidine suggested that this motif might be part of a METTL9 recognition sequence [42]. It was also observed that a single HxH is the minimal sequence motif required for METTL9-mediated methylation, although the methylation levels are higher when alternating histidine sequences are longer [42].
In the study by Lv et.al, 2021 [43] the middle residue was determined to be cysteine (C), alanine (A), glycine (G) or serine (S). The authors also note that the sequence containing alternating histidine residues corresponded to a x-His-x-His motif (xHxH-motif) [43], thus there is some dispute regarding the recognition motif of METTL9. Nonetheless, both groups agree that the motif is built up of alternating histidine residues separated by a small and uncharged residue [42, 43]. This reported motif corresponds well to the comprehensive proteomics analysis by Kapell and Jakobsson [36] from 2021, where a similar sequence motif was noted as being overrepresented in proteins with histidine methylation.

In addition to the recognition sequence, several *in vitro* and *in vivo* substrates have also been identified for METTL9. Both *in vivo* and *in vitro* substrates are summarized in Table 1 of the study by Davydova et.al [42]. Six substrates have been identified as being methylated *in vivo*, and METTL9 dependance has been formally demonstrated for three of these, namely NDUFB3, S100A9, and ZIP7 (SLC39A7) [42, 44]. S100A9 is an immunomodulatory protein, and this protein was known to contain 1MH modifications already in 1996 [47].
NDUFB3 is an accessory subunit of mitochondrial Complex I and Davydova et.al demonstrated that METTL9 mediated methylation of NDUFB3 enhanced respiration via Complex I [42]. In addition, a ZIP7-derived peptide containing multiple HxH-motifs showed a decreased affinity for zinc in the methylated (relative to the unmethylated) state [42].

ZIP7, encoded by the gene SLC39A7 (Solute Carrier family 39 member 7), is a zinc transporter of the ZIP family responsible for exporting zinc from the ER to the cytoplasm [48]. In addition to ZIP7, multiple peptide sequences derived from other zinc transporter proteins have been identified as *in vitro* substrates of METTL9, see Table 1 of the study by Davydova et.al [42].
In a study by Daitoku et.al, 2021 [44] the effect of METTL9 mediated methylation of the immunomodulatory protein S100A9 was investigated. S100A9 has a zinc binding site, and when an unmethylated S100A9-derived peptide was compared with its methylated counterpart, observations were similar as to those for ZIP7 [42], with zinc binding being significantly reduced for the methylated peptide [44].
For both ZIP7 and S100A9 this suggest that METTL9-mediated methylation modulates their zinc-binding ability in some way [42, 44]. Seeing as the residues targeted by METTL9 in

S100A9 are involved in metal coordination, and the 1MH modifications of the ZIP7-derived peptide showed reduced zinc binding, the potential role of METTL9 in regulating the homeostasis of metal ions such as zinc should be further investigated.

1.6 Zinc transporters

The regulation of cellular proliferation, metabolism and cell signaling are all cellular processes with one thing in common: they require zinc to function properly [49, 50]. In addition to being a vital mineral, zinc is also a very important second messenger and a vital regulator of gene expression [49, 50]. Zinc cannot freely pass through the membrane of cells and intracellular organelles [51], and for this reason mobile zinc is highly regulated, primarily by a class of multi-pass membrane proteins known as zinc transporters [52].

In mammals, these zinc transporters are divided into two classes known as the ZIPs/SLC39As and the ZnTs/SLC30As [53]. In loops or in the vicinity of the N-terminus, most zinc transporter proteins contain histidine-rich stretches which are studded with HxH-motifs, most often referred to as histidine-rich regions [53] (see Figure 5). In combination with previously reported METTL9 substrates being proteins involved in metal coordination, this makes zinc transporter proteins very interesting as potential substrates of METTL9 [42].

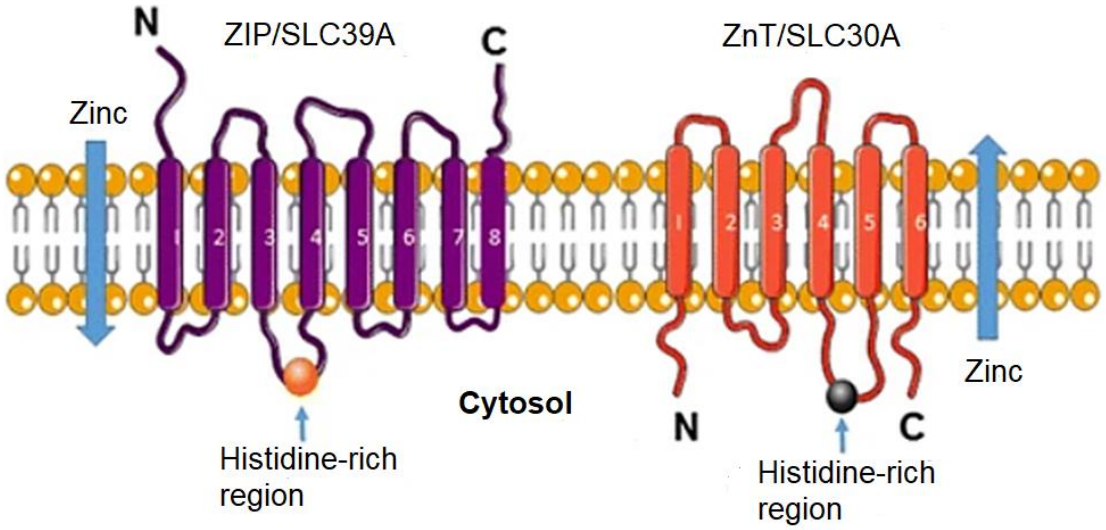

Figure 5: Predicted structures of the two families of zinc transporters. ZIPs are predicted to have 8 transmembrane domains (TMDs) with the histidine-rich region (red ball in figure 5) between TMD 3 (III) and 4 (IV). ZnTs are predicted to have 6 TMDs, with the histidine-rich region (black ball in figure 5) between TMD 4 (IV) and 5 (V). Figure adapted from [54].

In humans, the **ZIP family**, also referred to as SLC39As (Solute Carrier family 39) in literature, consists of 14 members to date [53]. ZIPs predominately localize to various membranes where they serve to import zinc from the extracellular environment and organelles into the cytosol of cells thus increasing the concentration of zinc in the cytosol [53]. The ZIPs are predicted to

have 8 transmembrane domains (TMDs) with a histidine-rich region between TMD 3 (III) and 4 (IV), as can be seen in Figure 5.

The **ZnT family**, also referred to as SLC30As (Solute Carrier family 30) in literature, will be the main focus for the duration of this introduction.
This family includes 10 proteins to date, 9 of which have been firmly established to operate as zinc transporters [53]. Zinc transporters belonging to this family are predominantly predicted to form homodimers, and are found in the membranes of intracellular organelles and serve to export zinc from the cytosol and into organelles or to the extracellular environment [53]. ZnTs thus serve to decrease the concentration of zinc in the cytosol. Based on 3D structures of YiiP, an *Escherichia coli* and *Shewanella oneidensis* ZnT homologue, the ZnTs are predicted to have 6 TMDs, with a histidine-rich (his-rich) region not found in YiiP between TMD 4 (IV) and 5 (V) as can be seen in Figure 5. The function of this his-rich region is not yet fully elucidated, but several theories exist. An additional ZnT-specific feature is the sequence of the N-terminus. In a study by Fukue et.al [55] from 2018, it was noted that this N-terminal region could regulate zinc transport via an interaction with the histidine-rich region, but that ZnT family members are likely functional even if the N-terminal region is absent.

1.6.1 ZnT-family transporters ZnT5 and ZnT7

A lot of enzymes require zinc for proper function, and many of these zinc-requiring enzymes become functional during their transport along the secretory pathway. Examples of such enzymes are matrix metalloproteinases, which are important for numerous biological processes such as cellular proliferation and modification of the extracellular matrix during development [56], angiotensin-converting enzymes, which plays an important role in regulating blood pressure [57] and alkaline phosphatases also known as ALPs, who contribute to hydrolyzation of phosphate groups from different molecules and are essential for bone mineralization [58]. Zinc transporters responsible for importing zinc into the lumen of the secretory pathway, therefore have important roles.
ZnT5, ZnT6 and ZnT7 all belong to the ZnT family of zinc transporters and have been identified as locating to the early secretory pathway, with both ZnT5 and ZnT7 predominantly showing localization to the Golgi apparatus, but some reports also indicate them as being located in the ER [59-63]. Interestingly, the ZnT-specific N-terminal region is particularly long in ZnT5 where it consists of 410 amino acids, which is not homologous to any other members of the ZnT family [60]. The function of this sequence is thus far not clear, but as is not cleaved proteolytically, it is thought to serve an important function [61]. It's long, N-terminal portion give ZnT5 an additional nine TMDs (and a total of 15 TMDs) which are fused to the carboxy-terminal

half of the other canonical six TMDs, which are found in all ZnTs [61, 64]. This makes ZnT5 a much larger transmembrane protein than the other members of the ZnT family.

ZnT5 normally operates in a heterodimer with ZnT6, as opposed to the typical homodimers predominantly formed by the ZnT-family transporters [65]. ZnT6 has a serine-rich region in the place of the his-rich region typically found in all zinc transporters [61]. ZnT5 functions as the essential component of the dimer and the his-rich region of ZnT5 is indispensable for both zinc transport activity and dimer formation, whereas ZnT6 is catalytically inactive [61]. ZnT6 only has one HxH-motif, the preferred motif targeted by METTL9 for 1MH methylation, and thus this zinc transporter is less likely to be regulated by METTL9. The remainder of this introduction will therefore be focused on ZnT5 and ZnT7 whose his-rich regions is displayed in Figure 6.

(A) His-rich region in ZnT5 (aa 542-592)

...HAHSHAHGASQGSCHSSDHSHSHHMHGHSDHGHGHSHGSAGGGMNANMRGV...

(B) His-rich region in ZnT7 (aa 162-236)

...GGHGHSHGSGHGHSHSLFNGALDQAHGHVDHCHSHEVKHGAAHSHDHAHGHGH
FHSHDGPSLKETTGPSRQILQ...

Figure 6: Histidine-rich regions in sequences from mammalian ZnT5 and ZnT7. Demonstration of potential methylation sites targeted by METTL9. Alternating histidine motifs in the form HxH have been underlined and highlighted (in blue). Lone histidine residues (not part of an HxH-motif) has been colored in red. Figure has been made using mammalian sequences from UniProt. Accession number, ZnT5: Q8TAD4. Accession number, ZnT7: Q8NEW0.

Cells lacking ZnT5-ZnT7 display similar cellular zinc contents as that of wild type (WT) cells, and thus their main function is providing zinc to zinc-requiring enzymes biosynthesized in the early secretory pathway [61]. An example of such zinc-requiring enzymes is a group of glycosylphosphatidylinositol (GPI)-anchored membrane proteins known as alkaline phosphatases or ALPs whose function is entirely reliant on zinc ions bound in their active site. This zinc is predominantly provided by ZnT5-ZnT6 heterodimers and the ZnT7-ZnT7 homodimers [51]. In humans, ALPs are found in most tissues and is often upregulated in various diseases, thus serving as an important biomarker in clinical evaluations [61]. Other zinc-requiring enzymes, both secretory and extracellularly located, are also dependent on zinc-loading by ZnT5-ZnT7 for both activity and expression [66].

As a further demonstration of their importance, when ZnT7 is knocked out in mice on a defined diet, this leads to zinc deficiency and decreased weight gain [67] as well as sex-dependent effects on the gut cell composition [68]. When ZnT5 is knocked out in mice, the mice display abnormalities in bone development and sudden death due bradyarrhythmia, meaning a slower than normal heart rate [69].

Interestingly, elevated expression of several SLC30A genes, including the genes encoding the ZnT5 and ZnT7 proteins, are related to better overall survival of patients with gastric cancer [70]. In addition, the median expression levels of the same zinc transporter genes are upregulated in gastric cancer tissues compared to normal tissue [70]. This suggests that in the future zinc transporters might serve a purpose as predictive biomarkers for patients with gastric cancer. If a number of these zinc transporters in addition are seen to be methylated by METTL9, once the function of METTL9 mediated methylation of zinc transporters have been further elucidated, METTL9 might also serve a purpose as a potential biomarker.

1.7 Aim of Study

The purpose of the study described in this thesis was to experimentally investigate an interesting subset of potential substrates of the recently characterized histidine-specific MTase, METTL9, namely zinc transporter proteins. For this purpose, genes encoding the zinc transporters ZnT5 and ZnT7 were PCR-amplified and subsequently cloned into plasmids for expression GFP-tagged proteins. GFP-tagged zinc transporters where then overexpressed in human cell lines via both stable and transient transfection. Cell lysates were then checked for expression of GFP-tagged zinc transporters using Western Blotting and METTL9 mediated methylation was investigated via an MTase assay with results being checked by fluorography. Methylation content in GFP-tagged zinc transporters was then analyzed via AAA.

2. Materials and methods

2.1 Cloning of ZnT5 and ZnT7

The plasmids used for cloning were the pEGFPC1 and the pEGFPN1 plasmids for mammalian expression of N-terminally and C-terminally tagged proteins respectively. The DNA fragments to be cloned were the ZnT5 (SLC30A5) and ZnT7 (SLC30A7) protein coding sequences. Both pEGFPC1 and pEGFPN1 contain a gene conferring resistance to Kanamycin (antibiotic) as well as Neomycin (antibiotic). Kanamycin was used for selection in bacterial cells whilst G418/Geneticin which is an analog of Neomycin, was used for selection in mammalian cells.

2.1.1 Generation of cDNA

cDNA to be used as template for amplification of ZnT5 and ZnT7 was prepared from the three following wild type (WT) cell lines: HeLa, HAP1 and TREx. Cells were grown in 75 cm^2 tissue culture flasks (VWR), until the cells had reached ~50% confluency, then harvested by trypsinization and the cell pellet was collected as described section 2.2.2 and 2.2.3 respectively.

Isolation of RNA

The RNeasy Mini Kit was used to purify and isolate the RNA extracted from cell pellets. The protocol “Purification of Total RNA from Animal Cells Using Vacuum/Spin Technology” from the RNeasy Mini Handbook (10/2019) was used following procedure 1b. At step 3, option 3c was followed thus the lysate was passed five times through a blunt 20-gauge needle (0.9mm in diameter, BD Microlance) fitted to an RNAse-free syringe prior to proceeding to step 4.
Deviations from the protocol include centrifuging the samples at 10,000 x g for 30 seconds prior to proceeding from step 10 to step 11. In addition, prior to collecting the flowthrough at step 13, the RNeasy spin column was centrifuged at 10,000 x g for 2 minutes. Step 15 was performed a total of two times, to ensure a higher concentration of eluted RNA.
Following RNA extraction, concentrations were measured using the Nanodrop 2000, in order to accurately determine how much extracted RNA was needed for subsequent cDNA synthesis.

cDNA synthesis via reverse transcription

SuperScript™ III Reverse Transcriptase (Invitrogen) was used and the “Frist-Strand cDNA Synthesis” protocol (as provided with the Reverse Transcriptase) was followed to transcribe the extracted RNA into cDNA. A total of 2.5 µg of RNA was used for all three cell lines

mentioned in section 2.1.1 “Generation of cDNA”. Deviations from this protocol include using 0.5 µl of oligo$(dT)_{20}$ (100µM) primer and the exclusion of RNaseOUT™ Recombinant RNase Inhibitor. Apart from this, the protocol provided with the SuperScript™ III Reverse Transcriptase (Invitrogen) was followed strictly.

2.1.2 PCR

To amplify DNA sequences for ZnT5 and ZnT7 with primers suitable for cloning into the pEGFPC1/N1 plasmids, standard polymerase chain reactions (PCR) with Phusion Polymerase (NEB) were run using the cDNA, gel-purified PCR product or plasmid DNA as template. Templates used for PCR amplification are described in the section “PCR templates for amplification of ZnT5 and ZnT7”.

Following the Phusion Polymerase protocol, 20 µl PCR reactions were prepared containing 4µl 5X HF (High-fidelity) buffer, 0.4 µl 10mM dNTP Mix, 1 µl template (~250 ng cDNA, ~10 ng PCR product, and ~100 ng for plasmid, see section “PCR templates for amplification of ZnT5 and ZnT7”), 2µl 10 µM primer mix (see section “PCR primers for amplification of ZnT5 and ZnT7”), and 0.2µl HF Phusion polymerase. H_2O was used to adjust total volume of the PCR reaction to 20 µl.

The PCR reactions were mixed gently via pipetting and placed in a C1000 Touch™ Thermal Cycler (BioRad). See Appendix, PCR program 1, 2 and 3 for full overview of cycles used for amplification.

PCR samples were loaded on gel and gel-extracted as described in section 2.1.4.

PCR templates for amplification of ZnT5 and ZnT7

Initially, cDNA from HeLa cells and TREx cells were used as templates for PCR amplification of ZnT5 and ZnT7 (following PCR program 1 as listed in the Appendix). Due to minimal results using cDNA from HeLa cells as template, this was replaced with cDNA from HAP1 cells for subsequent PCRs (following PCR programs 1 and 2, Appendix).

It was also attempted to use PCR product obtained using PCR program 2 (Appendix) as template for the amplification of both ZnT5 and ZnT7 in order to increase amplified product. PCR program 3 (Appendix) was followed when PCR product was used as template for amplification.

For the amplification of ZnT5, pDONR221_SLC30A5 plasmid was ordered from Addgene to serve as template for PCR amplification. PCR program 3 (Appendix) was followed when plasmid was used as template for amplification of ZnT5. For the amplification of ZnT7 in the pEGFPC1 plasmid, ZnT7 cloned into the pEGFPN1 plasmid was used as template. PCR program 3 (Appendix) was followed when plasmid was used as template for amplification of ZnT7.

PCR primers for amplification of ZnT5 and ZnT7

Prior to any physical lab work, primers were designed for human ZnT5 (SLC30A5) and human ZnT7 (SLC30A7) sequences. This was done using the canonical protein isoform from UniProt. Accession Number, human ZnT5: Q8TAD4 (Q8TAD4-1, canonical sequence). Accession Number, human ZnT7: Q8NEW0. In addition, the CCDS from NCBI was used to get the cDNA sequence. CCDS Accession number used for human ZnT7: CCDS776.1. CCDS Accession Number used for human ZnT5: CCDS3996.1.

Both forward and reverse primers were then designed using parts of the cDNA sequence for each of the two genes, and the primers were then adjusted for cloning in frame into the following plasmids: pEGFPC1 and pEGFPN1. Finalized primers can be found in the Appendix. Primer stocks for amplification of ZnT5 and ZnT7 were made at 100 µM. Using 2.5 µl of the primer stock made of the forward (FWD) primer and 2.5 µl of the primer stock made of the reverse (RV) primer, a primer mix was made for a total volume of 25 µl (adjusted using H_2O). For each gene to be amplified, a total of two primer mixes were made, one for cloning into the pEGFPC1 plasmid, and one for cloning into the pEGFPN1 plasmid.

2.1.3 Generation of linearized vectors

For the purpose of cloning, pEGFPC1 and pEGFPN1 were linearized with restriction enzymes BamHI and XhoI as follows.

For each plasmid, a single colony was picked from Kanamycin (50 µg/ml)-containing Luria Broth (LB) agar plates containing DH5α *Escherichia coli* (*E.coli*) cells transformed with either pEGFPC1 or pEGFPN1. The colonies were placed in 5 ml LB medium with Kanamycin (50 µg/ml) and incubated in a shaking incubator (37ºC) over night. Overnight (ON) cultures were then miniprepped as described in section 2.1.8.

In order to linearize the two miniprepped plasmids, the plasmids were digested with restriction enzymes XhoI and BamHI. A 50 µl digestion reaction was made using ~10 µg DNA, 5µl Cutsmart buffer and 1 µl of each restriction enzyme.

Reaction samples were heated for 1 hour at 37ºC to ensure sufficient digestion by XhoI and BamHI. Digested samples were loaded on gel and subsequently gel-extracted as according to section 2.1.4.

2.1.4 Gel electrophoresis and gel extraction

Agarose gel electrophoresis was used to verify PCR amplified sequences as well as generated linearized plasmids. Loading dye (6x, VWR) was added to the samples (amount used corresponded to 1/5th of sample volume) for visualization of bands under UV-light. Samples

were run on a 1% agarose gel containing 2.5 µl/50 ml GelRed® Nucleic Acid Gel Stain (Biotium) in 1xTAE buffer (Appendix) for 30 minutes, 100 V. To estimate sizes of DNA fragments observed on the gel, two GeneRuler ladders (1 kB and 100 bp) (Invitrogen) was loaded on each gel.

The gel was viewed under UV-light and bands corresponding to expected sizes were cut out using a scalpel. DNA from gel slices was extracted using the "DNA, RNA, and protein purification: NucleoSpin®: Gel and PCR clean-up" kit (Macherey-Nagel), according to protocol 5.2 "DNA extraction from agarose gels". DNA concentrations were measured using Nanodrop 2000. Isolated and extracted DNA was stored at -20ºC until further use.

2.1.5 In-Fusion cloning

In order to create constructs expressing C-terminally and N-terminally tagged ZnT5 and ZnT7, PCR amplified ZnT5 and ZnT7 were cloned into the pEGFPC1 and pEGFPN1 plasmids using In-Fusion cloning (Takara Bio).

In-Fusion cloning requires that a 15 nucleotide (nt) sequence homologous to the ends of the linearized plasmid is designed at the ends of primers used for amplification of the DNA fragment to be inserted into said plasmid [71, 72]. This ensures that the linearized plasmid and the insert have homologous ends [71, 72]. When the fragment and the linearized plasmid are incubated together with the In-Fusion enzyme mix (Takara Bio) the enzyme mix removes nucleotides from the 3' end of the DNA strands, creating overhangs [71, 72], as can be seen in Figure 7. This leads to spontaneous annealing of overlapping complementary DNA overhangs allowing for the unidirectional insertion of the fragment into the plasmid [71, 72].

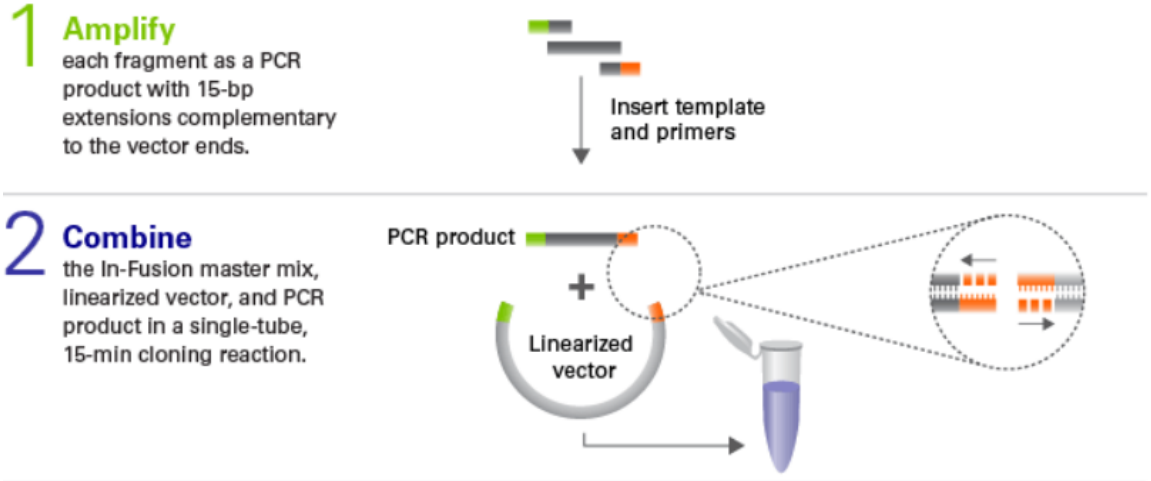

Figure 7: Schematic overview of the In-Fusion cloning method (Takara Bio). Figure is adapted from Takara Bios website [73]. Recombinant plasmid (constructs) was made using PCR product and linearized plasmid (referred to as "vector" in this figure) as according to figure 7.

In-Fusion reactions were made to a total volume of 5 µl with following contents: 1 µl 5X In-Fusion® HD enzyme Premix (Takara Bio), ~50 ng of the linearized plasmid (either pEGFPC1

or pEGFPN1) and ~50 ng of PCR-amplified insert (ZnT5 or ZnT7). Reactions were mixed in a PCR tube (VWR) and volume of In-Fusion reaction was adjusted using H_2O. Two In-Fusion reactions were made per PCR-amplified insert: one for cloning into the pEGFPC1 plasmid and one for cloning into the pEGFPN1 plasmid.
The In-Fusion reactions were incubated at 50ºC for ~30 minutes.

2.1.6 Transformation of DH5α *E.coli* cells

Constructs made using In-Fusion cloning were combined with 50 µl competent DH5α *E.coli* cells in order to transfer constructs into bacterial cells. Prior to isolation of DNA via midiprep (see section 2.3.1), miniprep samples prepared in section 2.1.8 were combined with 6 µl DH5α *E.coli* cells. Once the In-Fusion reaction or miniprep sample had been added to the DH5α cells, samples were incubated on ice for 20 minutes, followed by heat-shock (42ºC for 45 seconds) and then a cool down on ice for ~1-2 minutes. 200 µl Super Optimal broth with Catabolite repression (SOC) medium (Takara Bio) was added to the samples under a fume hood, before the samples were incubated in a shaking incubator for 1 hour at 37ºC. When miniprep samples were transformed into DH5α *E.coli* cells, 100 µl SOC medium (Takara Bio) was used.
Transformed *E.coli* cells were spread on LB agar plates with Kanamycin (50 µg/ml) for selection of positive transfectants. The plates were then incubated at 37ºC overnight and checked for surviving colonies the following day.

2.1.7 Inoculation of bacterial colonies

Prior to isolation of DNA by miniprep (see section 2.1.8, “Isolation of DNA (miniprep)”), a selection of surviving colonies (between 2 and 4 colonies per construct) were picked and transferred to Falcon tubes containing 5 ml LB medium with 5 µl Kanamycin (50 µg/ml). The Falcon tubes were incubated overnight in a shaking incubator at 37ºC. The following day, overnight cultures were miniprepped according to section 2.1.8.
Prior to isolation of DNA by midiprep (see section 2.3.1, “Isolation of DNA (midiprep)”), 1 surviving colony per construct was picked and transferred to Falcon tubes containing 10 ml LB medium with 10 µl Kanamycin (50 µg/ml) and incubated over night at 37ºC in a shaking incubator. In order to upscale for the purpose of midiprep, the following day the inoculation was transferred to larger bottles with 300 ml LB medium and 300 µl Kanamycin (50 µg/ml) and incubated over night at 37°C in a shaking incubator.

2.1.8 Isolation of DNA (miniprep)

In order to extract and isolate DNA, the “DNA, RNA and protein purification NucleoSpin® plasmid” kit (Macherey-Nagel) was used following the “5.1 Isolation of high-copy plasmid DNA

from *E.coli*" protocol with minor deviations. Deviations for provided protocol include that steps 4 and 5 ("Bind DNA" and "Wash silica membrane" respectively) were performed using a vacuum manifold (QIAGEN) and not centrifugation.
For step 7, where DNA was eluted, 30 µl Buffer AE was used when eluting constructs and 50 µl Buffer AE was used when eluting the empty pEGFPC1/-N1 plasmid.
Post-elution of minipreps, DNA concentrations were measured using the Nanodrop 2000.

2.1.9 Sequencing and analysis of sequencing results

~1 µg of the isolated DNA along with 2,5 µM sequencing primer (Appendix) were combined and the sample volume was adjusted to 10 µl with H_2O. The resulting sequencing sample was then sent off for analysis at EUROFINS.
In order to analyze sequencing results obtained from EUROFINS, the sequences were downloaded in the .ab1-format and pasted into the BioEdit program. If the resulting chromatogram showed a single, strong sequence, the FASTA format of said sequence was obtained and pasted into a file. The program Expasy was then used to translate the FASTA sequence into its resulting amino acid sequence and then Muscle alignment was used to align the cDNA sequence from UniProt with the amino acid sequence from Expasy (from the sequenced sample).
Linker sequences for both pEGFPC1 plasmid and pEGFPN1 plasmid were checked to ensure that the insert (gene) had been cloned in-frame with the GFP-tags expressed by pEGFPC1 and pEGFPN1.

2.2 Human cell culture

Mammalian cells were grown in a monolayer at 37°C and 5 % CO_2 in various flasks, tissue culture dishes or wells of different sizes, depending on amount of cells needed for the procedure to be performed.

2.2.1 Medium

HAP1 cells were cultured in Iscove's Modified Dulbecco's Medium (IMDM) (Gibco). TREx-293, HeLa and HEK293T cells were cultured in Dulbecco's Modified Eagle's Medium (DMEM) (Gibco). Complete IMDM and DMEM medium contained 50 ml Fetal Bovine Serum (FBS) per 500 ml medium as well as 50 U/ml penicillin and streptomycin (P/S) (Gibco, 5,000 U/ml).

2.2.2 Passaging cells

To prevent cell lines from overgrowing, cells were frequently passaged. Prior to passaging cells, cellular confluency was observed under a light microscope. If passage was deemed

appropriate due to high cellular confluency, medium was removed, and cells were washed with phosphate buffered saline (1xPBS) (Invitrogen) and subsequently detached using 0.05% Trypsin-EDTA (1X, Gibco). 5 ml 1xPBS and 1.5 ml 0.05% Trypsin-EDTA where used for cells grown in T75-flasks (VWR), whilst 20 ml 1xPBS and 5 ml 0.05% Trypsin-EDTA where used for cells grown in T182-flasks (VWR). 5 ml 1xPBS and 1 ml 0.05% Trypsin-EDTA was used when cells were plated on 100 mm tissue culture dishes (VWR) whilst 2-3 ml 1xPBS and 500 µl 0.05% Trypsin-EDTA was used when cells were plated on 6-well cell culture plates (VWR). Single colonies grown on 24-well cell culture plates (VWR) were washed using 1 ml 1xPBS, and 200 µl 0.05% Trypsin-EDTA was used to detach cells.

Incubation to achieve adequate trypsination of cells was performed in an incubator at 37ºC (with 5 % CO_2) for 5-10 minutes. Depending on cell line being passaged, appropriate medium (listed in section 2.2.1) was added to the mixture of trypsin and detached cells, and cells were resuspended by pipetting to homogenize the mixture. Amount of medium for resuspension in different cell culture vessels was as follows: 15 ml medium for T-182 flasks (VWR), 8.5 ml medium for T-75 flasks (VWR), 4 ml medium for 100 mm tissue culture dishes (VWR), 2.5 ml medium for 6-well cell culture plates (VWR) and 800 µl medium for 24-well cell culture plates (VWR).
An aliquot of the resulting cell suspension was then transferred to a new cell culture vessel pre-filled with fresh medium (12 ml in T75 flasks, 35 ml in T182 flasks, 3 ml in 6-well cell culture plates and 12 ml for 100 mm tissue culture dishes). Amount of cell suspension transferred varied depending on desired confluency in new cell culture vessel. To verify cellular presence in the new cell culture vessel, the vessel was inspected under a light microscope. Passaged cells were then placed in an incubator at 37ºC (with 5 % CO_2) and cellular confluency was closely monitored.
Note that medium, trypsin and PBS was always pre-warmed prior to being used for cell passage.

2.2.3 Generation of cell pellet

Cells were washed and trypsinated as described in section 2.2.2. Post-incubation with 0.05% Trypsin-EDTA (1X, Gibco), cells were resuspended in complete medium before being transferred to a 50 ml Falcon tube. 4 ml complete medium was used when cells were plated on 100 mm tissue culture dishes (VWR), and 2 ml complete medium was used when cells were plated on 6-well cell culture plates (VWR).
Note that detached cells plated on 100 mm tissue culture dishes (VWR) used for subsequent GFP-trap were resuspended in 4 ml ice-cold 1xPBS, not complete medium.

Cell suspension was then centrifuged at 400 x g for 5 minutes, 4°C. Supernatant was discarded post-centrifugation, and 1xPBS (Invitrogen) was added to the cell pellet. 5 ml 1xPBS was added to cells plated on 100 mm tissue culture dishes, whereas 2 ml 1xPBS was added to cells plated on 6-well cell culture plates. Cells were resuspended and centrifuged at 400 x g for 5 minutes, 4°C. Supernatant was discarded, and pellet was resuspended in 1 ml 1xPBS. Resuspended cell pellet was then transferred to pre-chilled 2 ml freezing tubes and centrifuged at 400 x g for ~7-10 minutes, 4°C. PBS was discarded via suction leaving only pellet in the freezing tubes.

2.2.4 Freezing and thawing cells

Cell stocks were frozen in DMSO (Sigma) for further use. Cells were washed, trypsinated and resuspended as described in section 2.2.2. Resulting cell suspension was added to 50 ml Falcon tubes and centrifuged at 400 x g for 5 minutes, 4ºC. Following centrifugation, supernatant was discarded and freezing medium consisting of complete medium with 10% DMSO was added to the cell pellet. Pellet was resuspended in freezing medium by pipetting, and resuspended cells (~1 ml) were added to 2 ml screw-cap freezing tubes. Freezing tubes were then stored at -80ºC in a Styrofoam box for ~24 hours prior to being transferred to a liquid nitrogen tank awaiting further use.

When cells were needed ~1 ml aliquots of cells frozen in liquid nitrogen were thawed in room temperature (RT) before being added to either 12 ml (T75 flasks, VWR) or 35 ml (T182 flaks, VWR) complete medium (see section 2.2.1). Cells were then passaged when deemed appropriate as according to section 2.2.2.

2.3 Generation of transfected cell lines (stable and transient)

Various cell lines can be transfected with recombinant plasmids via both stable and transient transfection. During a stable transfection the gene of interest is integrated into the host-cell genome and thus kept during subsequent cell divisions. During a transient transfection, the gene of interest is not integrated into the genome, but rather transiently maintained in the nucleus of cells and transfected DNA is only expressed for a short amount of time [74].

When working with cell lines that have been stably transfected there is no need to re-transfect the cells, which you have to do for transient transfections. For transfection of human cell lines, we attempted both stable and transient transfections.

2.3.1 Isolation of DNA (midiprep)

Overnight inoculations for midiprep (see section 2.1.7) were transferred to 400 ml plastic centrifuge bottles and centrifuged at 5,000 x g for 15 minutes (JA-10 rotor ID) in an Avanti™ J-25 centrifuge. Post-centrifugation, supernatant was discarded, and pellet was midiprepped as according to the "Plasmid DNA: NucleoBond® Xtra Midi/Maxi Plus" kit (Macherey-Nagel). The protocol 7.1 "High-copy plasmid purification (Midi/Maxi)" was followed with eluted DNA being concentrated using the NucleoBond® finalizers (step 7.3 "Concentration of NucleoBond® Xtra eluates with NucleoBond® Finalizers"). DNA concentrations were measured before and after using the finalizer for comparison. Final elute was stored at -20°C for further use.

2.3.2 Transfection

For transfection of constructs into competent human cells, a cellular confluency of ~40% was aimed for on the day of transfection. Cells where plated accordingly in advance on either 6-well cell culture plates (VWR) or 100 mm tissue culture dishes (VWR).
Both stably- and transiently transfected cells were incubated at 37ºC (with 5 % CO_2) for ~24 hours prior to being imaged in a ZOE Imager (BioRad) to verify successful transfection.

Cells grown on 6-well cell culture plates (VWR) were transfected as follows. When WT HAP1 and HeLa cells were stably transfected ~5 µg isolated DNA (see section 2.3.1) was diluted in 250 µl Opti-MEM medium (Gibco). 9 µl Lipofectamine®2000 Reagent (1 mg/ml) (Invitrogen) was diluted in 250 µl Opti-MEM and 250 µl diluted Lipofectamine®2000 was then added to the diluted DNA. This mixture was then incubated at RT for ~20 minutes before 500 µl of the mixture was added to the cells to be transfected. Mixture was added to the cells dropwise and clockwise. When WT and METTL9 KO HEK293T cells plated on 6-well cell culture plates (VWR) where transiently transfected, ~2 µg of DNA and 5 µl Lipofectamine®2000 Reagent (1 mg/ml) (Invitrogen) was used. Amounts of Opti-MEM as well as incubation times where otherwise kept the same.

In order to upscale the transfections, cells were plated on 100 mm tissue culture dishes (VWR). Again, a confluency of ~40% was aimed for on the day of transfection. When WT HAP1 and HeLa cells were stably transfected, ~20 µg isolated DNA (see section 2.3.1) was added to a 1.5 ml Eppendorf tube and diluted in 500 µl Opti-MEM medium (Gibco). 20 µl Lipofectamine®2000 Reagent (1 mg/ml) (Invitrogen) was diluted in 500 µl Opti-MEM medium (Gibco), and 500 µl of this dilution was added to each Eppendorf tube containing diluted DNA. Mixture of diluted DNA and diluted Lipofectamine®2000 Reagent (1 mg/ml) (Invitrogen) were incubated for ~20 minutes at RT, before 500 µl of said mixture was added dropwise and clockwise to competent cells. When HEK293T WT and METTL9 KO cells plated on 100 mm

tissue culture dishes (VWR) were transiently transfected, ~10 µg DNA and 15 µl Lipofectamine®2000 Reagent (1 mg/ml) (Invitrogen) was used. Otherwise, amounts and incubation were kept the same.
In addition to being transfected with GFP-tagged zinc transporters, cells were also transfected with an empty pEGFPN1 plasmid (using the same concentrations and amounts as described above), which was used as a GFP-control in most downstream experiments.

WT and METTL9 KO HEK293T cells transfected prior to imaging in Olympus microscope (see section 2.4.2) were grown to a confluency of ~40% on microscopy plates prior to being transiently transfected with GFP-tagged zinc transporters. 2.5 µL Lipofectamine®2000 Reagent (1 mg/ml) (Invitrogen) was diluted in 250 µL Opti-MEM (Gibco) and incubated at RT for ~10 minutes. ~1 µg DNA was diluted in 250 µL Opti-MEM (Gibco), and 250 µl of the diluted Lipofectamine®2000 Reagent (1 mg/ml) (Invitrogen) was added to diluted DNA. Again, the DNA and Lipofectamine®2000 Reagent (1 mg/ml) (Invitrogen) mixture was incubated at RT ~20 minutes prior to being added (dropwise and clockwise) to the WT and METTL9 KO HEK293T cells.

2.3.3 Selection using Geneticin

Selection medium used to select for positive transfectants was also made using complete medium (see section 2.2.1) and varying concentrations of antibiotics.
For both WT HeLa and WT HAP1 cells, we started with 500 µg/ml Geneticin/G418 (Gibco, stock: 50 mg/ml) in complete medium. Selection medium was replenished when required. The concentration of G418/Geneticin was upped to 1 mg/ml following minimal cell death of the WT HAP1 cells, whilst starting concentration was kept for the WT HeLa cells (500 µg/ml). Ultimately, this concentration was increased to 1 mg/ml for WT HeLa cells as well.
Transfected cell pool was ultimately frozen as described in section 2.2.4.

Clonal selection using only WT HeLa cells

1-3 colonies were picked per transfected construct using a cloning cylinder for harvesting single colonies and 100 µl 0.05% Trypsin-EDTA (Gibco) was used to detach said colony. Colonies were then placed in wells on a 24-well cell culture plate (VWR). 1ml selection medium was used (1 mg/ml G418/Geneticin). To verify cellular presence in the wells, the plates were inspected under a light microscope. Cells were monitored and selection medium was replaced when appropriate.
Seven days after colonies were picked and placed in wells on a 24-well cell culture plate, colonies were passaged to a 6-well plate for upscaled growth. For protocol see section 2.2.2.

2.4 Subcellular localization studies using microscopy

2.4.1 Staining of cells

WT and METTL9 KO HEK293T were transiently transfected with GFP-tagged zinc transporters as described in section 2.3.2. After overnight incubation, the cells were stained with 0.2 µg/ml Hoechst (all constructs, apart from glass slide to be used for ER-tracker) (Sigma-Aldrich) for visualization of the nuclei. In addition, METTL9 KO HEK293T cells transiently transfected with ZnT7-GFP was stained with 1 µM ER-tracker (Sigma-Aldrich). Cells stained with ER-tracker were not stained with Hoechst.

Once appropriate stains had been added to the cells on the glass slides, the cells were incubated for ~20 minutes at 37ºC (with 5 % CO_2) before the medium was removed, and 1 ml 1xPBS was used to wash the cells. 1 ml colorless DMEM (Gibco) was added to the glass slides containing the cells, and the cells were imaged in the Olympus FluoView microscope by Dr. Jędrzej Małecki as described in section 2.4.2. Due to time constraints, only C-terminally tagged ZnT5 and ZnT7 was imaged in said microscope.

Pilot to assess concentrations of stains

Prior to visualizing localization of GFP-tagged zinc transporters in the Olympus FluoView Microscope, a pilot to estimate concentrations required of cell stains was performed. Cells were plated on wells on a 6-well cell culture plate (VWR), 3 wells contained WT HEK293T cells, and 3 wells contained METTL9 KO HEK293T cells. Once confluency in the wells had reached ~85-90%, the WT and METTL9 KO HEK293T cells were stained with Hoechst (10 mg/ml) (Sigma-Aldrich) and ER-tracker (100 µM) (Sigma-Aldrich). Concentrations tested for Hoechst was 1 µg/mL and 0.2 µg/mL and concentrations tested for ER-tracker was 500 nM, according to Figure 8.

Figure 8: Overview of pilot staining of WT and METTL9 KO HEK293T cells. Wells are labelled with concentrations attempted for the two different stains.

From the pilot, it was discovered that since both Hoechst and ER-tracker stained blue, the ER-tracker was difficult to visualize as the Hoechst was too overpowering. A mock-transfection was thus run, using 1 µM and 5 µM ER-Tracker. For accurate transfection procedure, see transfection of WT and METTL9 KO cells prior to imaging in the Olympus microscope (section 2.3.2). It was deemed that cells stained with ER-tracker was not to be stained with Hoechst, as they both stained blue.

2.4.2 Imaging with Olympus Fluoview Microscope

Live cells were imaged by Dr. Jędrzej Mieczyslaw Małecki using an Olympus FluoView 1000 (Ix81) inverted confocal fluorescence microscopy system, equipped with a UPLSAPO 60x NA 1.35 oil objective (Olympus). The different fluorophores were excited at 405 nm (Hoechst and ER-tracker) and 488 nm (GFP), and Kalman averaging (n=3, sequential) was used to record multichannel images. The fluorescent signals emitted from GFP and Hoechst/ER-tracker were acquired through green and blue channels, respectively, and subsequently merged.

2.5 SDS-PAGE, Western Blotting, and Immunoprecipitation

2.5.1 Cell lysis

As according to section 2.2.3, cell pellet collected from transiently and stably transfected cells plated on 6-well cell culture plates (VWR) or 100 mm tissue culture dishes (VWR) were collected via centrifugation and concentrated to ~1 ml in a freezing tube. Generally, when cells were plated on 100 mm tissue culture dishes (VWR) 200 µL RIPA buffer (Appendix) was added to the collected pellet, whereas when cells where plated on 6-well cell culture plates (VWR)

100 µl RIPA buffer was used. When preparing lysates prior to performing the GFP-tap (see section 2.5.4) cell pellet collected from 100 mm tissue culture dishes (VWR) was lysed using 400 µl RIPA buffer.
Once RIPA buffer had been added to the cell pellet, freezing tubes were left on ice for 15 minutes before being centrifuged at max speed in an Eppendorf centrifuge (Centrifuge 5415 R) for 10 minutes. Post-centrifugation protein concentrations were measured.

It was also attempted to lyse cell pellet with NuPAGE® LDS sample buffer (4x) (Invitrogen). Transiently transfected cells plated on 100 mm tissue culture dishes (VWR) were collected and cell pellet was generated as described in section 2.2.3. 500 µl NuPAGE® LDS sample buffer (4X) (Invitrogen) was then added to said cell pellet and incubated on ice for 15 minutes before being centrifuged at max speed for 10 minutes in Eppendorf centrifuge (Centrifuge 5415 R). Lysate was then sonicated (5 x 20 seconds on/10 seconds off, 40% intensity) and protein concentrations were measured.
Cells lysed with both RIPA and NuPAGE® LDS sample buffer (4x) (Invitrogen) were stored at -80 ºC for further use.

2.5.2 SDS-PAGE

In order to separate proteins, a Sodium dodecyl sulfate-polyacrylamide gel electrophoresis (SDS-PAGE) was performed. Protein samples were reduced and denatured by the addition of Sample Reducing Agent (SRA) (10x) (Invitrogen) and NuPAGE® LDS Sample buffer (4x) (Invitrogen) before being heated at 75°C for 10 minutes. Note that when proteins in samples containing GFP-tagged zinc transporters were separated by SDS-PAGE, this heating step was omitted.

Samples were then loaded on an Invitrogen NuPAGE™ 4-12% Bis-Tris Gel (either 1.0 mm x 10 well or 1.0 mm x 15 well depending on number of samples to be run). 3.5 µl Precision Plus Protein™ Kaleidoscope Ladder (BioRad) was used to estimate band sizes. The gel was run in 1xMES running buffer (Appendix), for 35 minutes at 200V. The gel was then equilibrated in a small container along with 1xTransfer buffer including 10% methanol (Appendix).

2.5.3 Western Blotting (WB)

In order to verify the expression of the GFP-tagged zinc transporters in cells, a Western Blot (WB) was performed. As mentioned in section 2.5.2 proteins were separated via SDS-PAGE before resulting protein bands were transferred to a MilliporeSigma™ Immobilon™-FL membrane (Fisher Scientific).

1xTransfer buffer (Appendix) was added to a container along with four sponges and two Thermo Scientific™ Western Blot filter papers for soaking. The FL membrane was marked in the bottom left corner and then activated in 10% methanol (VWR chemicals) for ~1 minute prior to being rinsed in the container containing the 1xTransfer buffer (Appendix).
1xTransfer buffer (Appendix) was added to the bottom of the blotting chamber along with two of the four soaked sponges. The equilibrated SDS-PAGE gel (see section 2.5.2) was picked up using one of the two soaked filter papers which were placed on top of the two sponges previously placed in the blotting chamber. The additional soaked filter paper as well as the additional two sponges were then added on top of the gel before the top half of the blotting chamber was assembled, and the blotting chamber was added to the transfer box. The blotting program was run for 1 hour with 25 V.

Following blotting from the gel to the FL membrane, the membrane was stained with Ponceau S (Sigma-Aldrich) for ~ 1 minute and rinsed with water. The membrane was then rinsed 3-4 times with 2% acetic acid, and this was followed with water until the FL membrane was no longer pink. The membrane was then placed in 10% methanol (VWR chemicals) and taken out to dry before it was imaged, as a reference for protein load. The membrane was then placed into a 50 mL Falcon tube and rehydrated with 10% methanol (VWR chemicals), before the membrane again was rinsed with water.

To prevent unspecific binding of antibodies, a blocking buffer (Appendix) was added to the Falcon tube containing the membrane, before the tube was left on a Movil-Rod roller for 30 minutes at RT. Blocking buffer was removed, before 2.5 mL Odyssey block (Li-COR Biosciences™) and 2.5 mL TBS-T (Appendix) was mixed in a 50 mL Falcon tube along with the first anti-body, anti-GFP (α-GFP) from rabbit in a 1:1000-1:5000 dilution. This mixture was then added into the Falcon tube containing the blocked WB membrane and rolled over night at 4ºC.

The following day the antibody solution was removed, and the membrane was washed with 20 mL TBS-T (Appendix) for 2 minutes. This wash was repeated for a total of five washes before 2.5 mL Odyssey block (Li-COR Biosciences™) and 2.5 mL TBS-T (Appendix) was added to the Falcon tube along with the secondary antibody, anti-rabbit (α-rabbit), in a 1:10 000 dilution. This was then rolled at RT for 1 hour.
The antibody solution was then discarded before the membrane was washed with 20 mL TBS-T (Appendix) for 2 minutes. This wash was repeated for a total of five washes, and the membrane was then placed in 10% methanol (VWR chemicals) and taken out to dry before being imaged on the Li-COR machine.

2.5.4 Immunoprecipitation (GFP-trap)

GFP-tagged proteins to be analyzed by amino acid analysis (see section 2.7.2) were immunoprecipitated (IP) via GFP-trap.

Cells were initially lysed as according to cell lysis method described in subchapter 2.5.1 and was added to a pre-cooled tube. A dilution buffer (Appendix) was added to the pre-cooled tube along with the cell lysate. In order to equilibrate the GFP-trap_A beads (Chromotek) the tube containing said beads was tilted multiple times.

40 µl of the resulting bead slurry was pipetted into 1000 µl of the dilution buffer (Appendix), and the mixture was centrifuged at 3,000 x g for 3 minutes, 4ºC. Supernatant was discarded post centrifugation. Diluted lysate in the pre-cooled tube was then added to the equilibrated GFP-trap_A beads (Chromtek), and samples were incubated head-over-tail for 2 hours, 4ºC. Following incubation, the GFP-trap_A beads were collected via centrifugation at 3,000 x g for 3 minutes, 4ºC, and supernatant was discarded. The beads where subsequently resuspended in 1000 µl ice-cold dilution buffer (Appendix), and centrifuged at 2,500 x g, 3 minutes, 4ºC. Resuspension in ice-cold dilution buffer and subsequent centrifugation was repeated for a total of two times with supernatant being removed post-centrifugation.

Proteins in IP samples were separated by size via SDS-PAGE (see section 2.5.2) before being checked via WB (see section 2.5.3), to ensure correct substrate was present in the samples.

2.6. MTase activity assay

In order to investigate whether or not ZnT5 and ZnT7 were methylated by METTL9, a reaction containing purified GST-hsMETTL9 (see section 2.6.1), GFP-tagged ZnT5 and ZnT7 and radioactive-labelled SAM was made, and an SDS-PAGE was performed (see section 2.5.2). Resulting protein bands were transferred to a MilliporeSigma™ Immobilon™-FL membrane (Fisher Scientific) which was sprayed with EN3HANCE (Perk-Elmer). This spray contains a radioactivity-sensitive fluorophore which generates light from radioactivity (present in the ^{3}H-SAM used as a methyl donor) and resulting protein methylation can then be detected via fluorography, where membrane and an autoradiography film is placed together in a light-proof cassette for exposure of said film at -80°C.

2.6.1 Protein purification

Cell pellet of BL21 bacteria expressing *homo sapiens* METTL9 (hsMETTL9) protein tagged with Glutathione-S-transferase (GST) was dissolved in cold lysis buffer (~15 ml/500 ml culture) (Appendix), and then sonicated (5 x 20 seconds on/10 seconds off, 50% intensity) while

keeping samples on ice. Sonicated cell lysate was then further incubated on ice for 15 minutes post-sonication. The cell lysate was then cleared by centrifugation at 15,000 x g for 45 minutes, 4ºC (Ultracentrifuge, JA-14 rotor). Glutathione Sepharose 4B (Sigma-Aldrich) was washed in lysis buffer (5 ml per 1 ml slurry, mixed by inversion) and then centrifuged at 400 x g for 3 minutes. The supernatant of the cleared cell lysate was then added to the washed Glutathione Sepharose 4B (Sigma-Aldrich). Post-centrifugation of the resin, the supernatant was discarded. ~200 µl resin was used per 200 ml original cell culture to bind the cleared lysate to the resin. This step was done overnight at 4ºC on a roller.

The following day, the resin with bound lysate (recombinant GST-tagged hsMETTL9) was centrifuged at 500 x g for 5 minutes, 4ºC and the supernatant was discarded. The resin with the bound lysate was then washed a total of two times with ~50 ml Wash buffer containing Triton (Appendix) in a 50 ml Falcon tube (bulk purification). Lysate and resin were then transferred to a Poly-Prep® Chromatography Column (BioRad) on a vacuum-manifold (QIAGEN) with light vacuum. The resin was subsequently washed a total of two times with 10 ml Wash buffer without Triton (Appendix). The Poly-Prep® column was then removed from the vacuum-manifold, and 10 mL Elution buffer, pH 8.0 (Appendix) was added and the elute was collected by gravity-flow. The elute was then concentrated to ~200 µl via centrifugation at 4,500 x g and buffer exchange was then performed twice using 7 ml Storage buffer (Appendix) in Vivaspin20 MWCO 10 kDa columns (REF:VS2002) (Fisher Scientific).
Purified, eluted GST-hsMETTL9 was then stored at -20°C for further use.

2.6.2 Methyltransferase reaction (MTase reaction)

Prior to performing an MTase assay, dilutions of the purified GST-hsMETTL9 protein were made using different amounts of purified enzyme and storage buffer (Appendix). In order to calculate the concentrations of purified GST-hsMETTL9, three different dilutions were prepared. Sample 1 contained 5 µl of the purified GST-hsMETTL9 and 5 µl of the Storage buffer (Appendix). A second dilution contained 1.1 µl of the purified GST-hsMETTL9 and 9.9 µl of the Storage buffer (Appendix). The third dilution contained 1 µl of sample “1” and 9 µl of the Storage buffer. 10 µl was loaded of all three dilutions.

GST-hsMETTL9 dilutions were loaded onto an SDS-PAGE gel alongside Bovine Serum Albumin (BSA) of varying concentrations. Concentrations loaded of BSA was as follows: 2 µg, 1 µg, 0.75 µg, 0.5 µg and 0.25 µg. The concentration of the prep (purified GST-hsMETTL9) was estimated to be ~0.3 µg/µl, see results section 3.4.1.

A reaction to verify methylation by GST-hsMETTL9 was made using ~1.5 µg purified GST-hsMETTL9, 5 µl substrate (lysate containing GFP-tagged zinc transporters) and 1 µl ^{3}H-SAM (Perkin-Elmer, specific activity=~77-78 Ci/mmol) with 50 mM Tris pH 7.6.
The MTase reaction was incubated for 1 hour in a shaking heating block at 37ºC. SRA (10x) (Invitrogen) and NuPAGE® LDS (4x) (Invitrogen) was added to the samples prior to loading the samples on an SDS-PAGE gel as described in section 2.5.2.

2.6.3 Fluorography

Once the SDS-PAGE gel had been transferred to an FL membrane by blotting (see section 2.5.3 for blotting procedure), the resulting membrane was sprayed with EN3HANCE (Perk-Elmer) until the membrane was appropriately coated and then dried.
In a dark room, the dried membrane was added to a light-proof Kodak X-Omatic cassette (Kodak) along with a Kodak® autoradiography BioMax MS film (Sigma-Aldrich) which was added on top of said membrane. The light-proof cassette was then covered in aluminum foil and stored at -80ºC for exposure for a total of four weeks before the film was inspected for bands.

2.7 Amino acid analysis

2.7.1 Amino acid hydrolysis

Preparation of gel slice

Following SDS-PAGE using samples obtained via GFP-trap IP, the gel was stained with Coomassie (Simply-Blue™ Safestain (Novex), Cat no. LC6065), and bands of interest were cut out with a scalpel. Extracted gel slice was cut into smaller pieces prior to being transferred to the bottom of a hydrolysis tube.

200 µl 6M HCl was added to the bottom of a hydrolysis tube containing the sample (obtained as described above) under a fume hood. The tube plug was inserted and screwed down just enough to leave a small passageway between the plug and the glass at the stricture point of the hydrolysis tube. Once the tube was deemed secured, the vacuum source was added to the side arm of the hydrolysis tube and vacuum was applied. Once there was no air remaining in the hydrolysis tube, the unit (tube and plug) was sealed by slowly screwing the plug until it was flush with the glass surface at the stricture, which creates a white line at said stricture. The unit was flicked several times to ensure that the gel slices were completely immersed in HCl. The sealed hydrolysis tube was then left for ~24 hours in a heating block set to 110ºC.

The tube was then removed, and cooled to RT, before hydrolysate was collected with a glass pipette and transferred to a 1.5 ml Eppendorf tube. The Eppendorf tube with hydrolysate was then placed back in a heating block (50ºC) with the lid open. The open Eppendorf tube was left in the heating block for ~24 hours. Once HCl was completely evaporated, the hydrolysate was resuspended in 500 µl H_2O, and the sample was filtered through a 0.45 µm non-pyrogenic filter using a 10 ml HENKE-JECT® single-use syringe. Another 500 µl H_2O was then added to the syringe to flush out hydrolysate from the filter. Hydrolysate was collected in a 1.5 ml Eppendorf tube and labelled. Samples were kept at -20ºC prior to being sent off for analysis.

2.7.2 Amino acid analysis (AAA)

Samples compiled as described in sections 2.7.1 were sent off for analysis to Lars Haugen at NTNU. To normalize the results received from Lars, the amount of detected 1-methylhistidine (nM) and the amount detected of 3-methylhistidine (nM) was divided by amount detected of histidine (nM) (individually) and timed with 100. Obtained results are visualized in a graph in section 3.4.4 of Results.

3. Results

3.1 PCR and Cloning

In order to express GFP-tagged ZnT5 and ZnT7 in cells and analyze whether or not these proteins were methylated by METTL9, DNA constructs for their expression in mammalian cells were created. Forward and reverse primers were designed so that the genes of interest could be inserted into the pEGFPC1 plasmid (which expresses an N-terminally GFP-tagged protein) and the pEGFPN1 plasmid (which expressed a C-terminally GFP-tagged protein).

In order to create the constructs for expression of GFP-tagged ZnT5 and ZnT7, the two genes were initially amplified by PCR using cDNA from HeLa and TREx cell lines as template (PCR program 1, Appendix). When the PCR samples were run on a 1% agarose gel in 1xTAE buffer (Appendix), the resulting bands were weak and unspecific. cDNA from HeLa cells was therefore replaced with cDNA from HAP1 cells (PCR program 1, Appendix). Due to minimal improvement in terms of amplification, a gradient PCR was performed (PCR program 2, Appendix) in order to get a stronger and more specific product, and ZnT5 was amplified using primers for insertion into the pEGFPC1 plasmid, whereas ZnT7 was amplified using primers for insertion into the pEGFPN1 plasmid. The PCR samples were then checked again on a 1% agarose gel in 1xTAE buffer (Appendix), and the resulting gels can be seen in Figure 9.

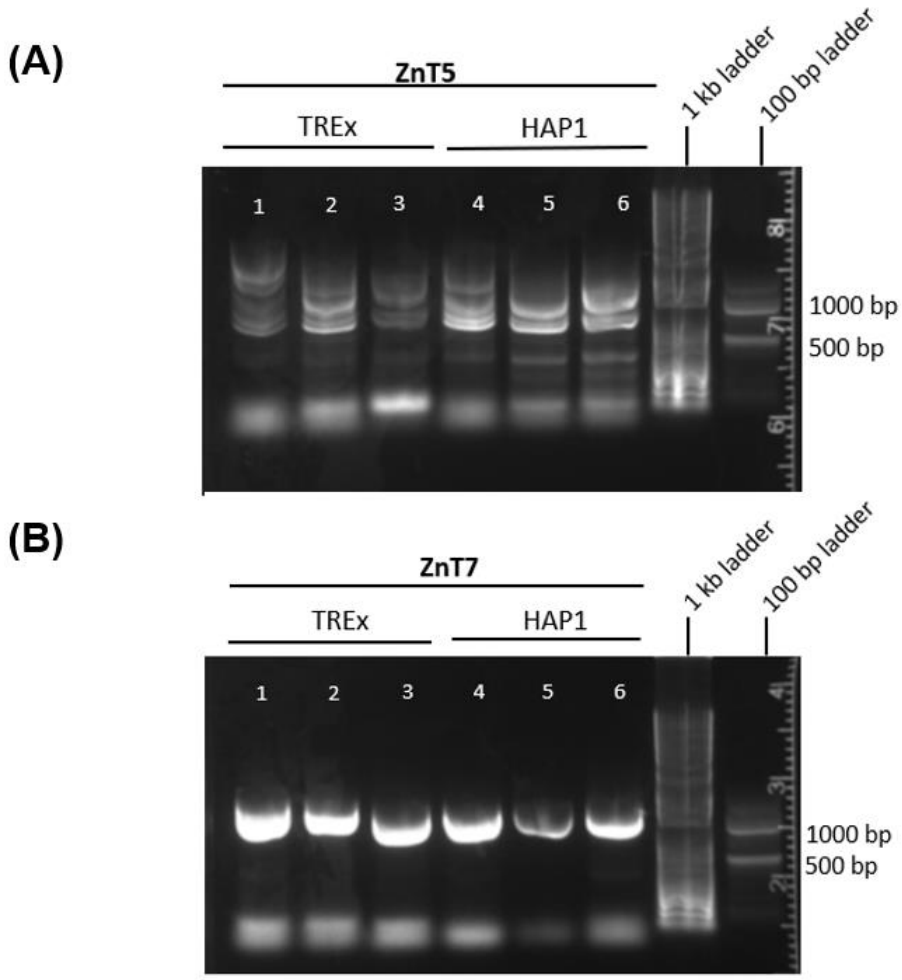

Figure 9: Gel pictures demonstrating result of PCR program 2 using cDNA from TREx and HAP1 as template for amplification. PCR results for the amplification of ZnT5 is shown in **(A)** and similarly is shown for ZnT7 in **(B)**. In both **(A)** and **(B)** a gradient was used for optimization of PCR. For the amplification of ZnT5 **(A)**, annealing temperatures used were 52.8ºC (lanes labelled 1 and 4), 51.1ºC (lanes labelled 2 and 5) and 49.7ºC (lanes labelled 3 and 6). Forward and reverse primers designed for cloning into the pEGFPC1 plasmid was used for amplification of ZnT5. For the amplification of ZnT7 **(B)**, annealing temperatures used were 65.5ºC (lanes labelled 1 and 4), 63.3ºC (lanes labelled 2 and 5) and 61.7ºC (lanes labelled 3 and 6). Forward and reverse primers designed for cloning into the pEGFPN1 plasmid was used for amplification of ZnT7. Excepted size of amplified ZnT5: 2.2 kb. Expected size of amplified ZnT7: 1.1 kb.

As can be seen in Figure 9 (B), ZnT7 showed an even amplification with one strong band of expected size (1.1 kb) using both TREx and HAP1 cDNA as a template source. This was displayed in all lanes (marked 1-6 in Figure 9, (B)). There was also little effect of changing the annealing temperature. PCR amplified ZnT5, Figure 9 (A), displayed multiple weaker bands of varying sizes with uneven separation.

From the two gels shown in Figure 9, the band closest in size to the expected size of ZnT5 (2.2 kb, band extracted from lane 4 in Figure 9 (A)) and ZnT7 (1.1 kb, band extracted from lane

2 in Figure 9 (B)) were gel-extracted and used as template for reamplification in order to increase the amount of PCR product (PCR program 3, Appendix), results not shown.

Following successful PCR amplification of ZnT7 (for pEGFPN1), and a somewhat successful PCR amplification of ZnT5 (pEGFPC1), the PCR products were cloned into the appropriate plasmids using In-Fusion cloning. The resulting minipreps were sequenced at EUROFINS to ensure presence of correct sequence. Sequencing showed that cloning was successful only for pEGFPN1-ZnT7.

For ZnT5, the sequencing results showed that none of the colonies picked for analysis contained a plasmid with the correct insert. This continued to be the case also when PCR product was used as template for amplification, and there was no strong product of expected size, and there were also no correct results upon sequencing. Reasons for this are unknown, but it could be that expression is low (or possibly entirely absent) in the cell lines we used as cDNA sources.

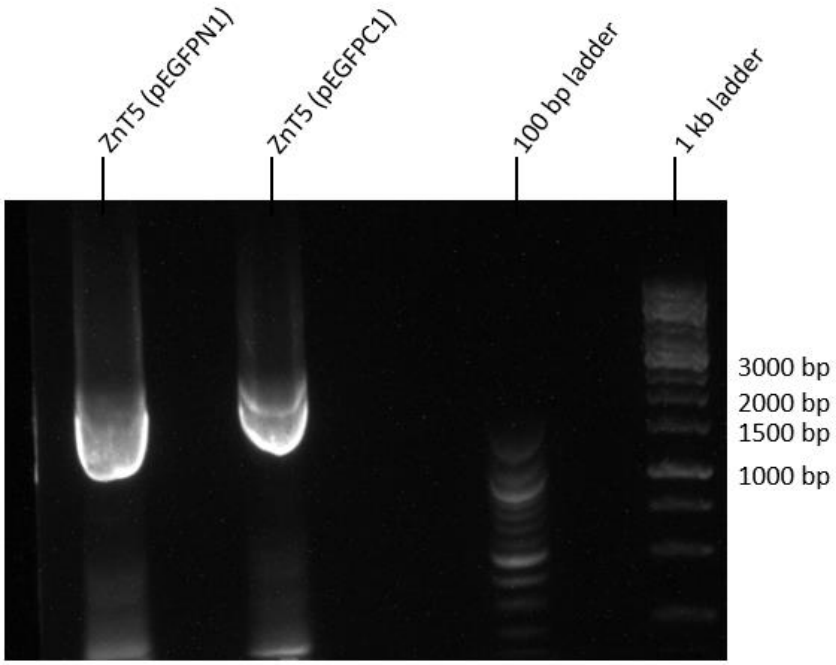

Figure 10: Picture of agarose gel demonstrating the PCR product of ZnT5 amplified using primers for insertion into the pEGFPC1 and pEGFPN1 plasmid using pDONR221_SLC30A5 plasmid (Addgene) as template. Resulting bands were gel-extracted and inserted into the pEGFPC1 and pEGFPN1 plasmids using In-fusion cloning. Expected size of ZnT5: 2.2 kb.

After previously mentioned attempts at cloning using PCR amplified ZnT5 yielded no results, a plasmid encoding the gene (pDONR221_SLC30A5) was ordered from Addgene. This plasmid was not suitable for our purposes and thus was only be used as template for PCR amplification of ZnT5 following PCR program 3 (Appendix). PCR samples were again run on a 1% agarose gel (in 1xTAE, Appendix), and the results of the amplification can be seen in

Figure 10. Bands observed give off a strong signal, and primer binding has been specific, though the bands are somewhat below expected size for ZnT5 (2.2kb), but this is likely due to the thickness of the bands. Both bands where gel-extracted and following cloning and sequencing the results finally showed successful amplification and cloning of ZnT5 into both pEGFPC1 and pEGFPN1 plasmids.

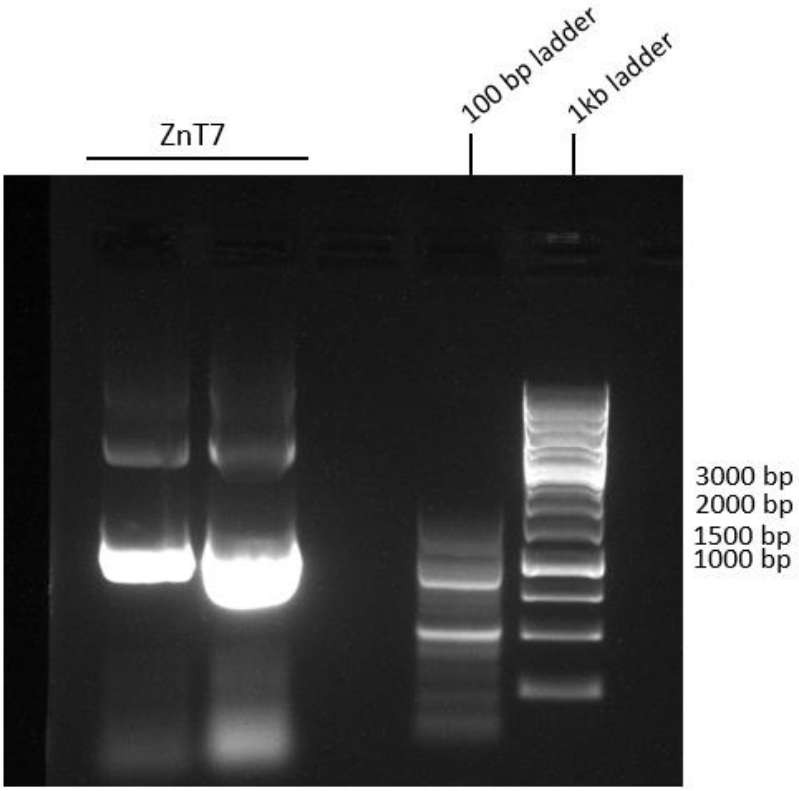

Figure 11: Picture of agarose gel demonstrating the PCR product of ZnT7 amplified using primers for cloning into the pEGFPC1 plasmid and the pEGFPN1-ZnT7 plasmid as template. Resulting bands were gel-extracted and cloned into the pEGFPC1 plasmid using In-Fusion cloning. Expected size of ZnT7: 1.1 kb.

For amplification of the ZnT7 sequence to be cloned into the pEGFPC1 plasmid, a miniprep of the pEGFPN1-ZnT7 plasmid was used as template for a PCR amplification. PCR program 3 (Appendix) was used for said amplification. Gel loaded with resulting PCR samples is shown in Figure 11. Both bands were extracted, and sequencing showed successful amplification and cloning of pEGFPC1-ZnT7.

Post-verification of sequences for ZnT5 and ZnT7, the constructs were again transformed into DH5α cells and colonies were selected for ON culture and subsequent inoculation in larger flasks, before a midiprep was performed. Midipreps give larger yields and purer DNA, which is more suitable for the following part, namely transfection and subsequent expression in human cell lines. Resulting midiprepped samples were also sequenced.

3.2 Protein expression in human cells

3.2.1 Stable transfection in HeLa WT and Hap1 WT cells

Using the pEGFPC1 and pEGFPN1 constructs encoding genes for ZnT5 and ZnT7, we initially attempted to create stably-transfected cell lines using WT HEK293T cells. Due to minimal cell death following selection with G418/Geneticin (analog of Neomycin), it was discovered that the cells used for transfection were resistant to G418/Geneticin, which is the antibiotic used for selection in human cells. Following this we used WT HeLa and WT HAP1 cells for stable transfection in subsequent experiments. Only WT cells were used initially in case setting up stably-transfected cell lines overexpressing GFP-tagged ZnT5 and ZnT7 proved unsuccessful. In addition, if neither ZnT5 nor ZnT7 were methylated in the WT cells, there would be no point in expressing the proteins in a METTL9 KO cell line.

Figure 12 (A) shows an example of ZnT5-GFP transfected into WT HAP1 cells and an example of the same construct transfected into WT HeLa cells can be seen in Figure 12 (B). In both cases the cells have been imaged in a ZOE Imager 24 hours post-transfection, meaning protein expression has occurred for ~24 hours prior to imaging the cells.

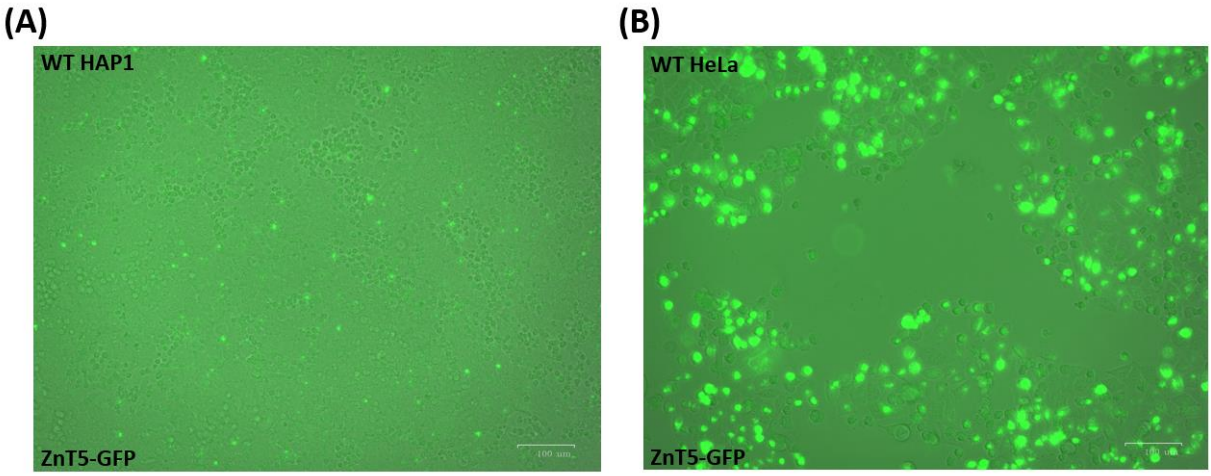

Figure 12: Expression of ZnT5-GFP post transfection in WT HAP1 cells (A) and WT HeLa cells (B) prior to being treated with Geneticin (G418). Cells were plated in 6-well plates, and protein was expressed for 24 hours prior to imaging in a ZOE Imager. Both (A) and (B) show merged images (Brightfield and green channels have been merged).

As can be observed in Figure 12 (A), when the constructs containing ZnT5 were transfected and subsequently expressed in WT HAP1 cells the transfection efficiency was very poor (~<10%). The transfection worked better for the WT HeLa cells, Figure 12 (B), with a resulting transfection efficiency of ~50%. After 2 days, growth medium was replaced with selection

medium (DMEM/IMDM + G148/Geneticin (500 µg/ml), see section 2.3.3 of Materials and Methods for further explanation) and cells were subsequently monitored for surviving colonies (results not shown). Old selection medium was replaced with new selection medium every couple of days, but cell death was minimal thus the amount of antibiotics was increased to 1 mg/ml, initially only for WT HAP1, but later also for the WT HeLa cells.

After a total of 20 days of selection using G418/Geneticin, several colonies had formed on the plates, and a number of surviving WT HeLa colonies were picked (1-3 colonies per construct) and passaged to individual wells on a 24-well cell culture plate (VWR) for clonal selection.

After 7 days, the single colonies were passaged to larger plates on a 6-well plate (VWR) and after 48 hours, colonies were collected and lysed for further analysis. In addition, we analyzed the remaining colonies as a pool. Surviving WT HAP1 colonies were also analyzed as a pool (no single clonal selection was attempted for this cell line due to colonies being too dense following treatment with antibiotics). Lysates were then made of both surviving individual colonies and pool (for WT HeLa cells) as well as pool for WT HAP1 cells and a small amount of the cell lines was kept in culture whilst protein expression was verified.

3.2.2 Verifying protein expression in WT HeLa and HAP1 cell lines via Western-Blotting

To analyze whether GFP-tagged ZnT5 and ZnT7 were expressed in either the pool of resistant cells (WT HeLa and WT HAP1 cells) or the selected clones (WT HeLa cells only) we used Western blotting of the cell lysates with an antibody against the GFP-tag. Results of said WBs are shown in Figure 13 (A) and Figure 14 (A), respectively.

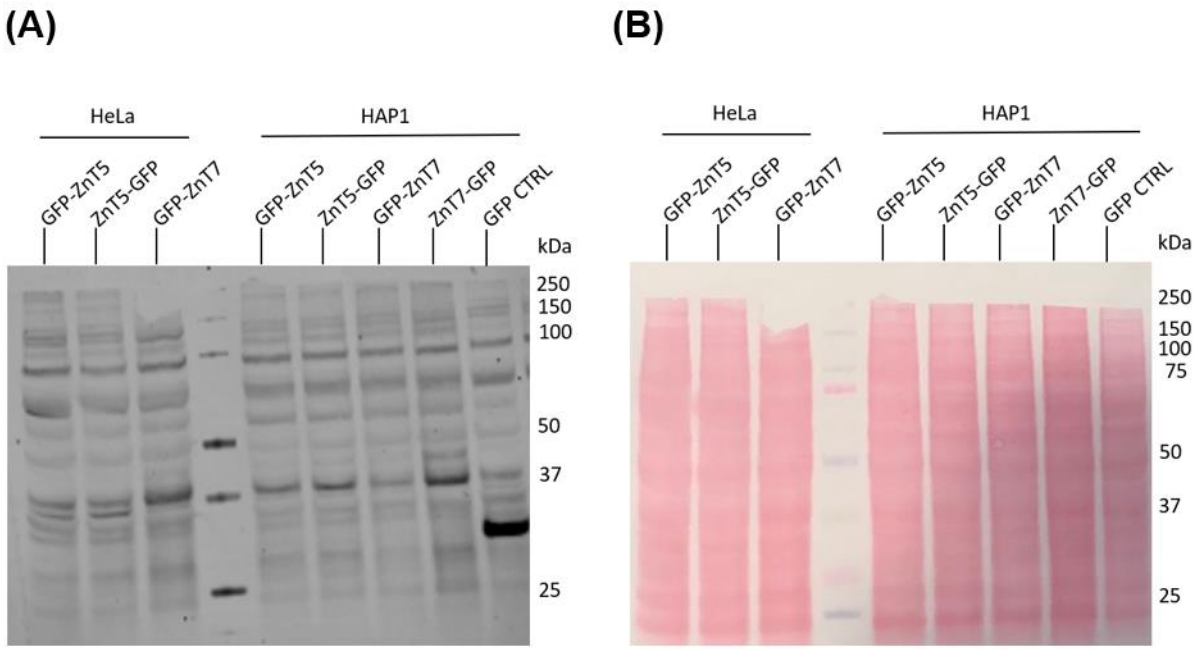

Figure 13: Western Blot showing expression of GFP-tagged ZnTs in WT HeLa and HAP1 cells (pool). Pool lysates from WT HeLa and WT HAP1 cells transfected with constructs encoding GFP-tagged zinc transporters **(A)**. The corresponding membrane stained with Ponceau S **(B)** is used as a reference for protein loading. Expected size of GFP-tagged ZnT5≈ 112,05 kDa. Expected size of GFP-tagged ZnT7≈ 69,6 kDa.

As can be seen from (A) in Figure 13, protein expression in WT HeLa and WT HAP1 cells could not be confirmed via Western Blotting using an anti-GFP antibody, as no specific signal was observed. There are weak bands which appear to be of expected size (GFP-tagged ZnT5≈ 112,05 kDa, GFP-tagged ZnT7≈ 69,6 kDa), but these bands can be found in all samples. In addition, there are multiple bands of varying sizes displayed on the membrane, which are also uniformly distributed amongst the different samples. As indicated by the stained membrane visualized in Figure 13 (B), this was not due to insufficient amount of lysate. Note that there is no lane containing lysates from WT HeLa cells expressing ZnT7-GFP in Figure 13 (A). The reason for this is that the plate containing cells expressing this construct was empty following treatment with G418/Geneticin, and thus it was not possible to collect any cell pellet containing this specific construct for this cell line. The WB in Figure 13 (A) does show that creation of stable cell line expressing GFP only (28 kDa) worked (marked with a red asterisk).

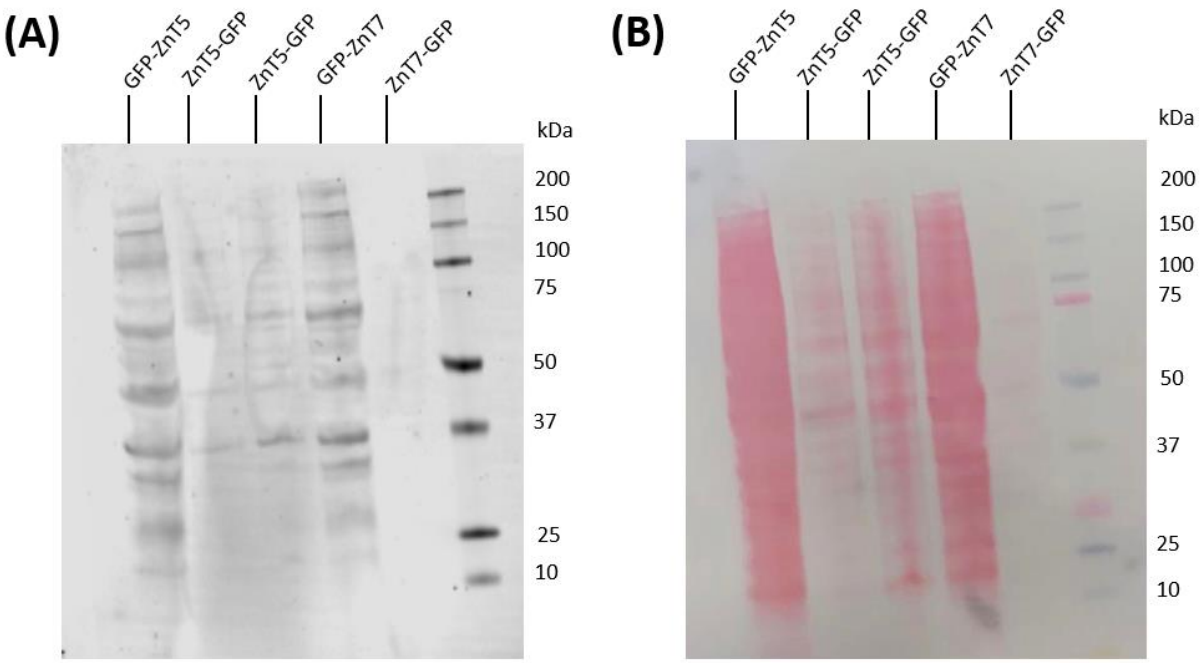

Figure 14: Western Blot showing expression of GFP-tagged ZnTs in WT HeLa cells (single colonies). (A) shows colony lysates from WT HeLa cells transfected with constructs encoding GFP-tagged zinc transporters. The corresponding membrane stained with Ponceau S (B) is used as a reference for protein loading. Expected size of GFP-tagged ZnT5≈ 112,05 kDa. Expected size of GFP-tagged ZnT7≈ 69.6 kDa.

Figure 14 (A) shows WB of cell lysates made from resistant clones of WT HeLa cells. Figure 14 (B) displays the membrane stained with Ponceau S as a protein load reference. Similar to the analysis of the lysates made from a pool of resistant colonies, the clonal lysates from WT HeLa cells did not confirm protein expression of the two GFP-tagged zinc transporters. Note here that the amount loaded, and hence the protein concentration, varied substantially between the samples, with N-terminally tagged ZnT5 and ZnT7 having a much higher concentration than their C-terminally tagged counterparts as can be seen in Figure 14 (B).

Both WBs (Figure 13 (A) and Figure 14 (A)) show a high degree of background and neither appear to contain any bands of the expected sizes. As mentioned, some lanes do actually contain bands of expected sizes, but these bands were also present in other lanes, so this does not confirm protein expression of desired constructs.

3.2.3 Transient transfection of WT and METTL9 KO HEK293T

We then decided that for further experiments, the GFP-tagged zinc transporters were to be transiently transfected in WT and METTL9 KO HEK293T cells. Initially cells were plated in wells of a 6-well cell culture plate (VWR), aiming for a confluency of ~50% upon time of transfection. Protein expression always occurred for 24 hours before the cells were imaged in a ZOE Imager. If the transfection efficiency was deemed appropriate (>20%, but cell pellet was

collected even with a lower transfection efficiency), cell pellet was collected, and cells were lysed for further analysis. Below is shown the initial result of all constructs transiently transfected into both WT and METTL9 KO HEK293T cells. Images were taken using the ZOE Imager (BioRad) and brightfield and green channels have been merged. Both WT and METTL9 KO HEK293T cells were always transfected in parallel with an empty pEGFPN1 plasmid, expressing GFP only, which served as a positive control (displayed in both Figure 15 and Figure 16).

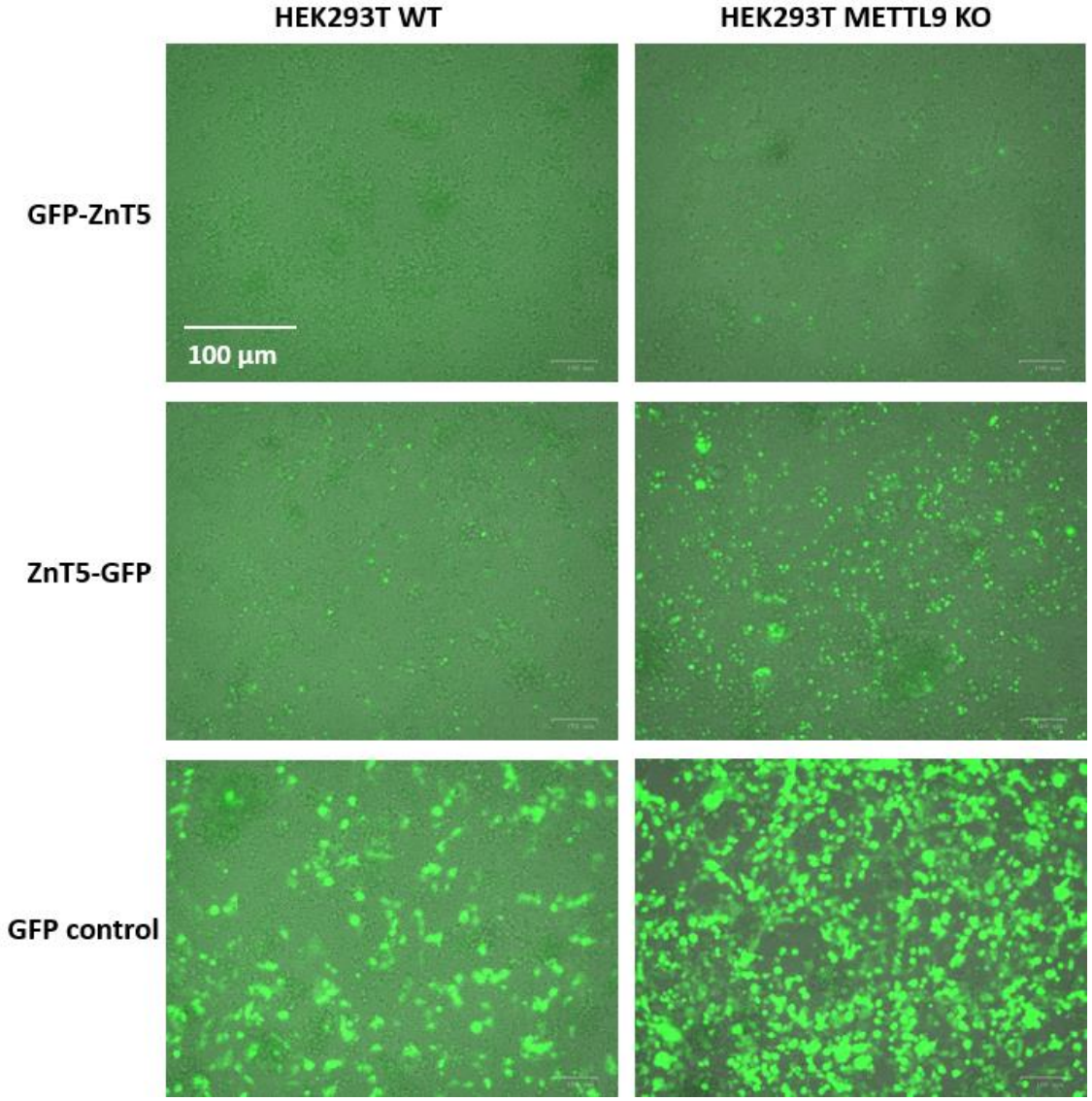

Figure 15: GFP-tagged ZnT5 transiently transfected in WT and METTL9 KO HEK293T cells. Cells have been plated on a 6-well cell culture plate (VWR) and transiently transfected with GFP-tagged ZnT5 (both C- and N-terminally tagged) before being imaged in a ZOE Imager (BioRad) ~24 hours post-transfection (24 hours of protein expression at the time the image was captured). HEK293T cells transiently transfected with an empty pEGFPN1 plasmid (expressing GFP only) was used as a positive control. For all six images shown, the magnification used on the ZOE Imager was the same (as indicated for GFP-ZnT5 transiently transfected in HEK293T WT cells), 100 µm.

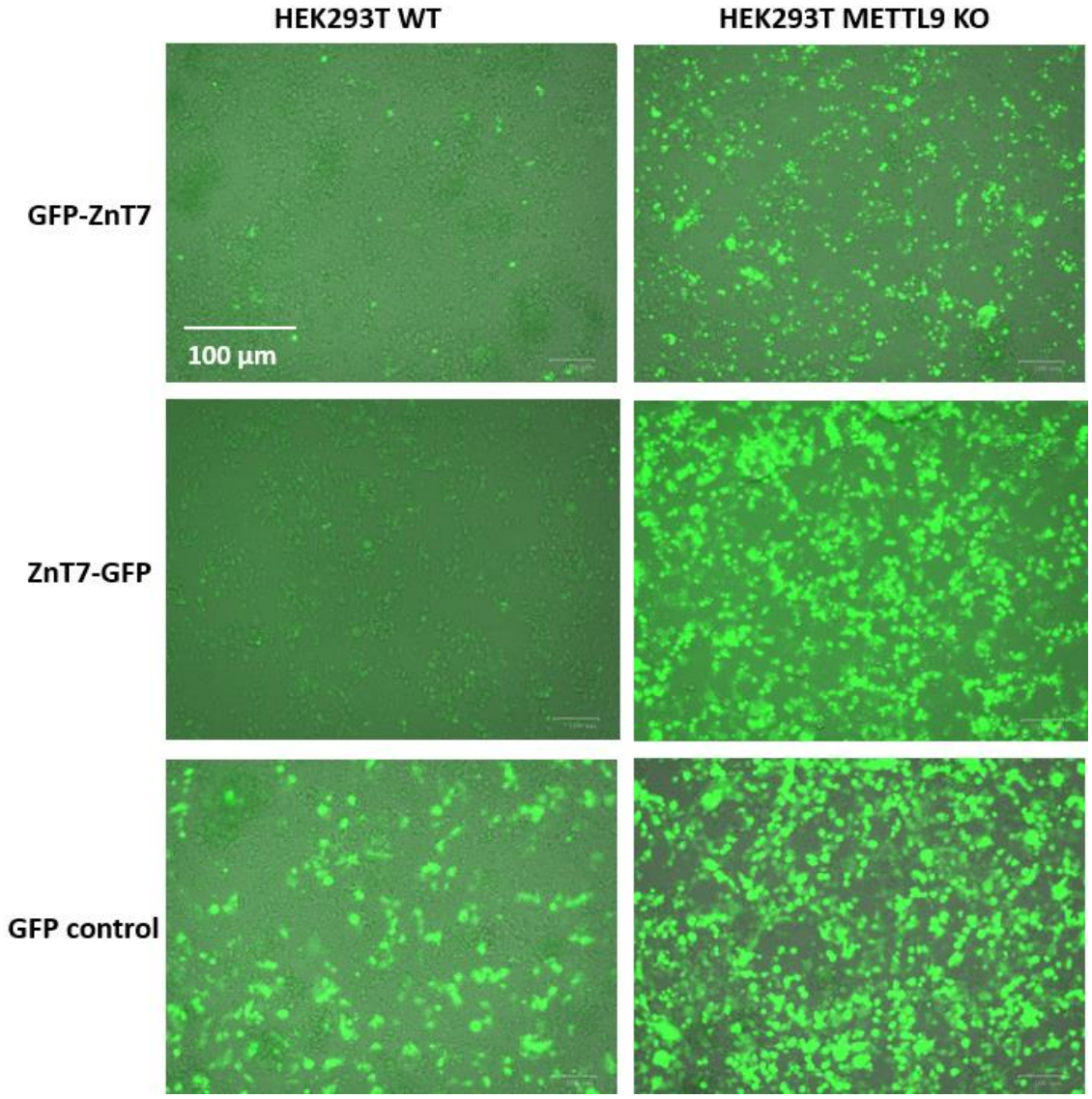

Figure 16: GFP-tagged ZnT7 transiently transfected in WT and METTL9 KO HEK293T cells. Cells have been plated on a 6-well cell culture plate (VWR) and transiently transfected with GFP-tagged ZnT7 (both C- and N-terminally tagged) before being imaged in a ZOE Imager (BioRad) ~24 hours post-transfection (24 hours of protein expression at the time the image was captured). HEK293T cells transiently transfected with an empty pEGFPN1 plasmid (expressing GFP-only) was used as a positive control. For all six images shown, the magnification used on the ZOE Imager was the same (as indicated for GFP-ZnT7 transiently transfected in HEK293T WT cells), 100 µm.

Transiently transfecting C-terminally and N-terminally tagged ZnT5 and ZnT7 in WT and METTL9 KO HEK293T cells showed an improvement in transfection efficiency compared to the same constructs being transfected into WT HAP1 cells, but not HeLa cells. As a general rule, for the multiple transient transfections performed using HEK293T cells (results of all transfections are not shown), the transfection efficiency was always better in METTL9 KO HEK293T cells, which can be seen in Figures 15 and 16, for both GFP-tagged zinc transporters

as well as for the expression of GFP only (GFP control). In addition, both C- and N-terminally tagged ZnT7 always showed a higher transfection efficiency than C- and N-terminally tagged ZnT5, and N-terminally tagged ZnT5 in most cases had the lowest transfection efficiency. This is true for when the construct was transiently transfected in WT HEK293T cells and METTL9 KO HEK293T cells.

3.2.4 Verification of protein expression in WT and METTL9 KO HEK293-T cells via Western Blotting

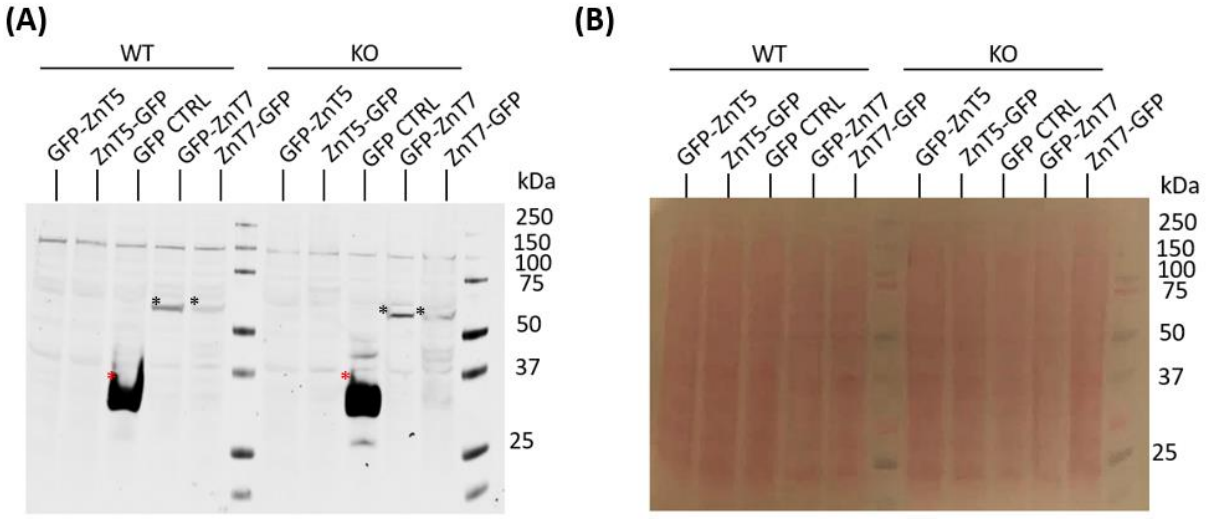

Figure 17: Western Blotting demonstrating overexpression of GFP-tagged ZnTs in HEK293T WT and METTL9 KO cells. Cells have been transiently transfected with constructs as indicated in (A) and (B). (B) shows the corresponding membrane stained with Ponceau S for reference on protein loading. Expected sizes for GFP-tagged ZnT7≈ 69.6 kDa. Expected size for GFP-tagged ZnT5≈ 112,05 kDa. Asterisk in (A) indicates confirmed expression of N- and C-terminally tagged ZnT7 (black) as well as GFP-control (red).

Following transient transfection of pEGFPC1 and pEGFPN1 constructs in WT and METTL9 KO HEK293T cells, definite expression of both N-terminally and C-terminally tagged ZnT7 was observed, as can be seen in Figure 17 (A). Confirmed protein expression was lower for C-terminally tagged ZnT7 compared to N-terminally tagged ZnT7. The expression also appears to be somewhat higher in the METTL9 KO cells compared to the WT cells, which corresponds well with what was seen in the ZOE Imager (see Figure 16).

As can be noted by the corresponding membrane stained with Ponceau S in Figure 17 (B), this does not clearly appear to be due to differences in protein loading. The stain does appear weaker for GFP-tagged ZnT7 samples from WT HEK293T cells compared to samples from METTL9 KO HEK293T cells, but this difference is minimal.

The expression of N-terminally and C-terminally ZnT5 could not be verified via Western Blotting as there were no bands of expected size (112,05 kDa).

Several other WBs were performed in order to see whether protein concentration in sample added on SDS-PAGE played a part in the displayed expression of ZnT5. In addition, it was attempted to replace lysing buffer (RIPA) for LDS, as it was suspected that perhaps due to ZnT5 being quite a large, TM protein with a total of 15 TMDs, it was ending up in protein pellet and thus being discarded as waste. Various amounts of lysate made from cells lysed with LDS instead of RIPA buffer was tested but this yielded no results (results not shown).

3.3 Functional studies in WT and METTL9 KO HEK293T cells

3.3.1 Visualization of C-terminally tagged Zinc transporter proteins transiently transfected in WT and METTL9 KO HEK293T cells

Subcellular localization of C-terminally tagged ZnT5 and ZnT7 transiently transfected in HEK293T cells, was studied using an Olympus FluoView microscope by Dr. Jędrzej Małecki, with resulting images displayed in Figures 18-20.
As can be seen in Figures 18 and 19, C-terminally tagged ZnT7 and ZnT5 seem to have similar distribution in both METTL9 KO and WT cell lines. This indicates that there is no difference in localization of these two C-terminally tagged proteins when METTL9 is present (WT) compared to when METTL9 is absent from the cells (METTL9 KO). However, in METTL9 KO cells, there appears to be a bit more aggregation.

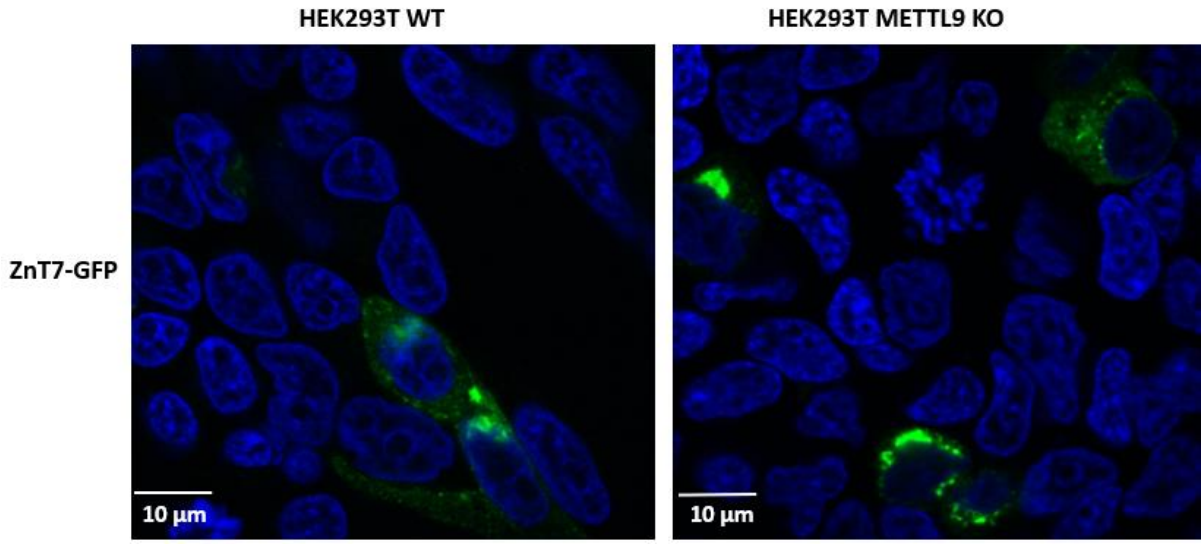

Figure 18: Visualization of C-terminally tagged ZnT7, transiently transfected in WT and METTL9 KO HEK293-T cells in order to observe localization of GFP-tagged zinc transporter. Cells have been stained with Hoechst (DAPI) to visualize the cell nuclei (blue), whereas the GFP fused to the protein is shown in green. Image taken using Olympus FluoView microscope by Dr. Jędrzej Małecki.

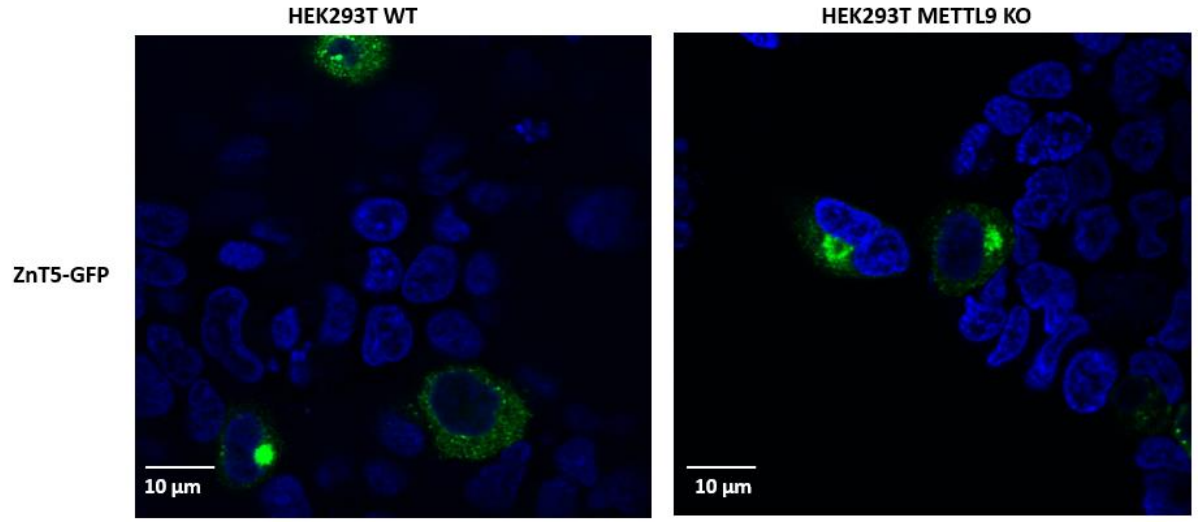

Figure 19: Visualization of C-terminally tagged ZnT5, transiently transfected into WT and METTL9 KO HEK293-T cells in order to observe localization of GFP-tagged zinc transporter. Cells have been stained with Hoechst (DAPI) for nuclei visualization (blue), and GFP-tag is displayed in green. Images taken using Olympus FluoView microscope by Dr. Jędrzej Małecki.

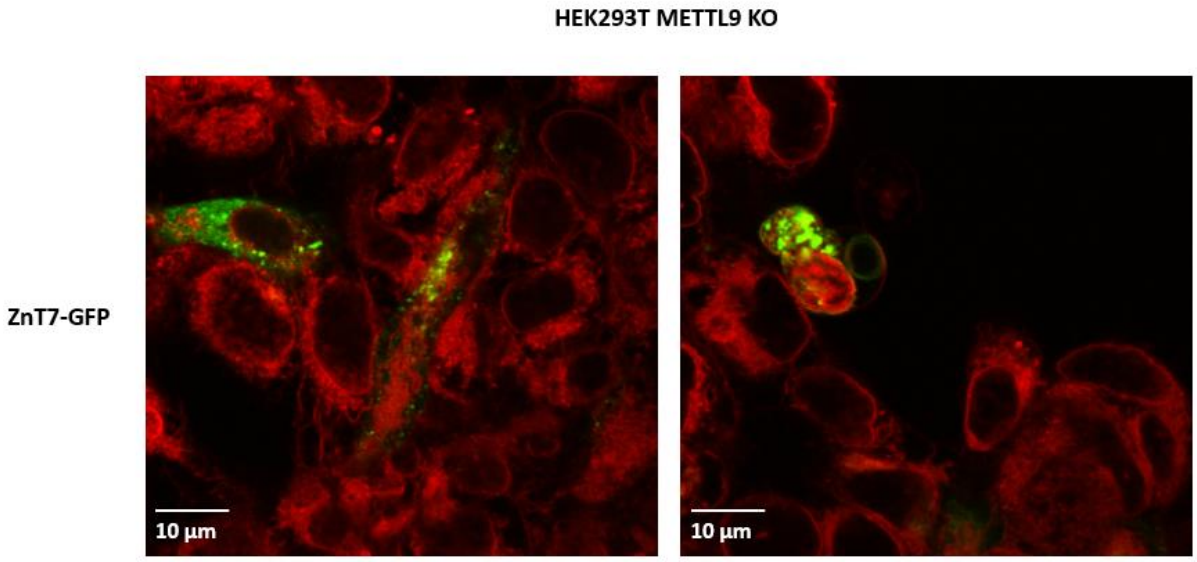

Figure 20: Visualization of C-terminally tagged ZnT7 expressed in METTL9 KO HEK293-T cells stained with ER-tracker (red). The GFP-tag is visible in green, and ER-tracker is visible in red. Images taken using Olympus Fluoview microscope by Dr. Jędrzej Małecki.

In both the METTL9 KO and the WT cells, ZnT7 (Figure 18) and ZnT5 (Figure 19) appear to localize to speckles surrounding the ER, which is most likely the Golgi apparatus or related vesicles. What these speckles are is not fully known, but they are consistent with the secretory pathway. Both ZnT5 and ZnT7 have been known to also localize to the ER [62, 63], but this could not be confirmed in this study, as can be seen in Figure 20, where METTL9 KO HEK293T cells transiently transfected with ZnT7-GFP have been stained with ER-tracker (Sigma-Aldrich). There appears to be some areas which might indicate overlap of ZnT7-GFP with the ER (yellow regions), but it is a bit difficult to tell.

It was attempted to also stain WT HEK293T transiently transfected with ZnT7-GFP with ER-tracker, but the transfection efficiency was rather low, and a lot of cells had detached, and therefore these images are not shown. It was not attempted to stain cells transiently transfected with ZnT5-GFP with ER-tracker.

3.4 Exploring methylation status of ZnT5 and ZnT7

In order to explore whether or not ZnT5 and ZnT7 are methylated by METTL9, both *in vitro* and *in vivo*, several experiments were performed to explore the methylation status of these proteins.

3.4.1 Approximating concentration of purified GST-hsMETTL9

In order to investigate whether GFP-tagged ZnT5 and ZnT7 expressed in HEK293T cells are subject to METTL9 methylation *in vitro*, an MTase assay was performed.

First, recombinant GST-hsMETTL9 was purified from bacteria, and its concentration was estimated using SDS-PAGE. Various concentrations of Bovine Serum Albumin (BSA) were run on the same gel with different dilutions of GST-hsMETTL9 and then the gel was stained with Coomassie (Figure 21). Expected size of BSA is 66.5 kDa and expected size of GST-hsMETTL9 is ~ 62.5 kDa (GST =26 kDa + hsMETTL9 = 36.5 kDa).

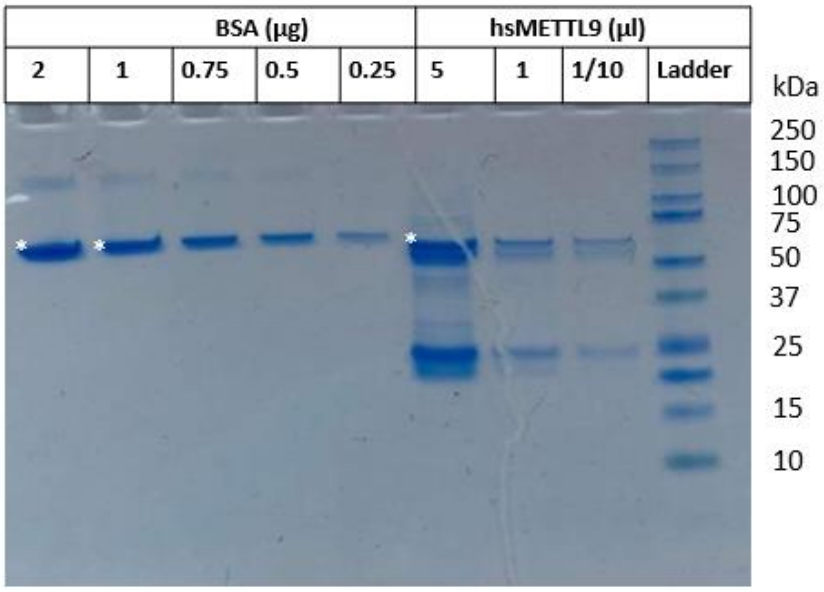

Figure 21: SDS-PAGE gel imaged post-staining with Coomassie. Varying concentrations of BSA was added to approximate the concentration of purified hsMETTL9 to be used for subsequent MTase assay. Concentrations of BSA loaded into each well is listed on the figure. Bands of BSA used to approximate concentration of GST-hsMETTL9 is marked with a white asterisk.

In order to calculate the concentrations of purified GST-hsMETTL9, three different dilutions were prepared, labelled as 5, 1 and 1/10 in Figure 21. Sample “5” contained 5 µl of the purified GST-hsMETTL9, sample “1” contained 1 µl of the purified GST-hsMETTL9 and sample “1/10” contained 1 µl of sample “1” meaning 0.1 µl of the purified GST-hsMETTL9. All samples were diluted using varying amounts of storage buffer (Appendix).

The band which contained 5 µl GST-hsMETTL9 (marked with a white asterisk in Figure 21) appeared similar to the band containing 2 µg BSA and to the band containing 1 µg BSA (both marked with white asterisks in Figure 21). It was therefore estimated that the amount in the 5 µl sample was 1.5 µg and thus the concentration of the purified GST-hsMETTL9 was estimated to be ~0.3 µg/µl.

3.4.2 MTase assay of lysates from HEK293T cells expressing zinc transporters, methylated with purified recombinant hsMETTL9

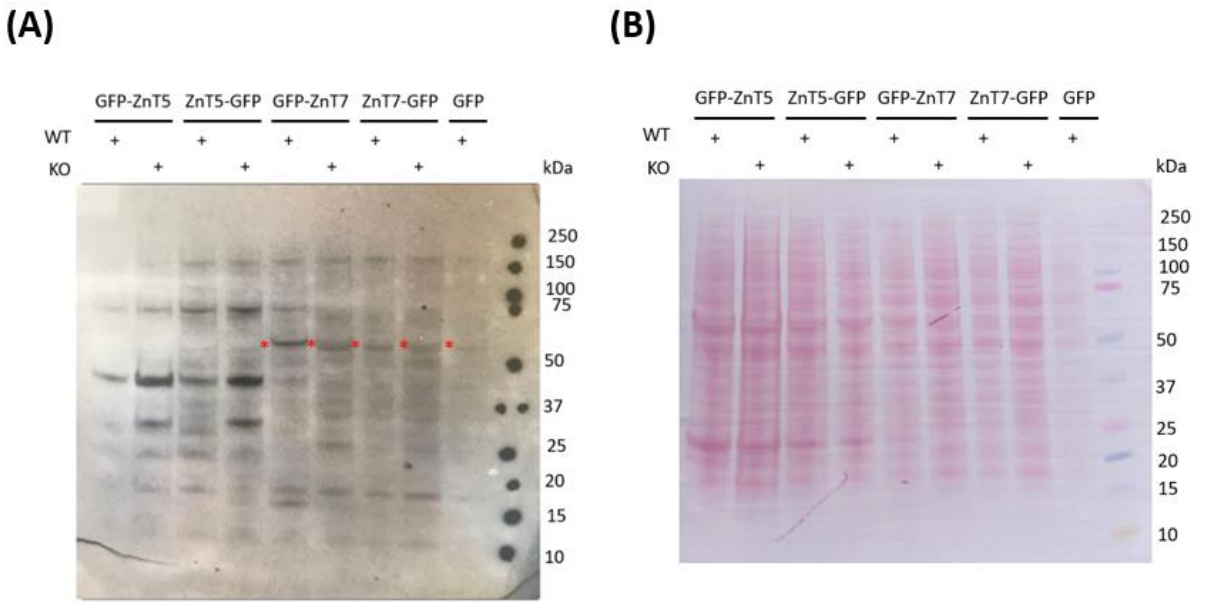

Figure 22: Fluorography and membrane of MTase assay where substrates have been incubated with purified recombinant hsMETTL9 and radioactive methyl donor. WT and KO represent cell lysates from either WT or METTL9 KO HEK293T cells expressing GFP-tagged transporters, which were used as substrates in the MTase assay. Expected size of ZnT7 fused with GFP ≈ 69.6 kDa. Expected size of ZnT5 fused with GFP ≈ 112.05 kDa. Red asterisk marks band of expected size for GFP-tagged ZnT7 proteins (in both WT and KO). (A) shows the developed fluorography film after four weeks of exposure and (B) shows the membrane stained with Ponceaus to visualize proteins.

The MTase assay was performed using 1.5 µg of GST-hsMETTL9 as the enzyme. ^{3}H-labelled SAM donor and 5 µl lysates from WT and METTL9 KO HEK293T cells expressing the different GFP-tagged zinc transporters (or GFP only as a negative control) as substrates. The reactions were separated by SDS-PAGE and transferred to a membrane. The membrane was stained with Ponceau S (Sigma-Aldrich), sprayed with an EN3HANCE spray (Perkin-Elmer) and exposed to an autoradiography film at -80°C. After a total of four weeks exposure, the fluorography film was developed and can be seen in Figure 22, (A)). The membrane stained with Ponceau S is displayed in Figure 22 (B) to visualize amount of protein loaded in the varying lanes.

Red asterisks on Figure 22 (A), marks bands corresponding in size to methylated GFP-tagged ZnT7 and thus confirms METTL9-mediated methylation of ZnT7 *in vitro*. A methylated band of this size is visible in the ZnT7 samples, regardless of which side the GFP-tag is on, and both in WT and METTL9 KO lysates. The ZnT7-GFP proteins appeared to be most weakly methylated by METTL9 compared to the GFP-ZnT7 proteins. In addition, and contrary to expectations, GFP-ZnT7 expressed in WT cells was a better substrate for METTL9 *in vitro* than in METTL9 KO cells. Note that the band representing GFP-tagged ZnT7 (marked with a red asterisk) also is visible in the lane containing the GFP-control (for WT HEK293T cells).

This is likely due to overflow from the previous lane which contained the ZnT7-GFP lysate from METTL9 KO cells. *In vitro* methylation of GFP-tagged ZnT5 could not be confirmed.

3.4.3 Immunoprecipitation and amino acid hydrolysis (AAH)

As no methylation could be observed for GFP-tagged ZnT5 following the MTase assay (see fluorography membrane in Figure 22 (A)), and its expression was undetectable by WB (Figure 17 (A)), only ZnT7 was used for further analysis.

In order to investigate methylation content in ZnT7, GFP-tagged ZnT7 transiently expressed in WT and METTL9 KO HEK293T cells was immunoprecipitated using GFP-trap. An empty pEGFPN1 plasmid expressing GFP-only was used also here as a control. Immunoprecipitated samples of C- and N-terminally tagged ZnT7 were then separated by SDS-PAGE, and a WB was performed to confirm presence of appropriate proteins. Both WB and corresponding gel can be seen in Figure 23 (A) and (B), respectively. Note that the order the samples have been loaded in is different for WT and METTL9 KO HEK293T cells (as indicated in Figure 23). This is due to a mix-up during the loading of the samples from the WT HEK293T cells. Therefore, contents of the wells, which can be seen in Figure 23, have been labelled correctly.

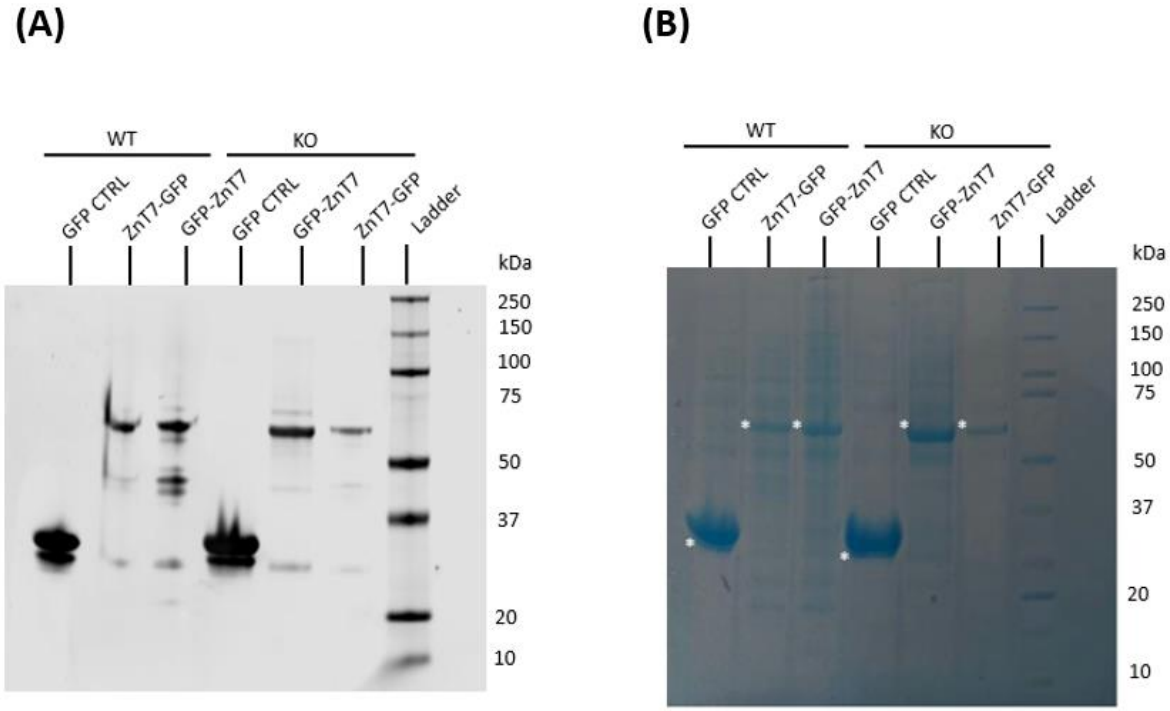

Figure 23: Western Blot and the corresponding SDS-PAGE gel displaying samples used for subsequent amino acid hydrolysis. (B) shows the SDS-PAGE gel post staining with Coomassie. Expected size of GFP-tagged ZnT7≈ 69.9 kDa. GFP-pulldowns of the indicated proteins from WT

HEK293T cells (WT) or METTL9 KO HEK293T cells (KO). Bands cut out and analyzed is indicated by white asterisk in (B).

Bands of appropriate sizes (marked with white asterisks) were cut out of the gel and subjected to acid hydrolysis to hydrolyze the proteins into amino acids. The samples were sent for amino acid analysis (AAA) at NTNU, and the results can be seen in Figure 24.

3.4.4 Amino acid analysis (AAA)

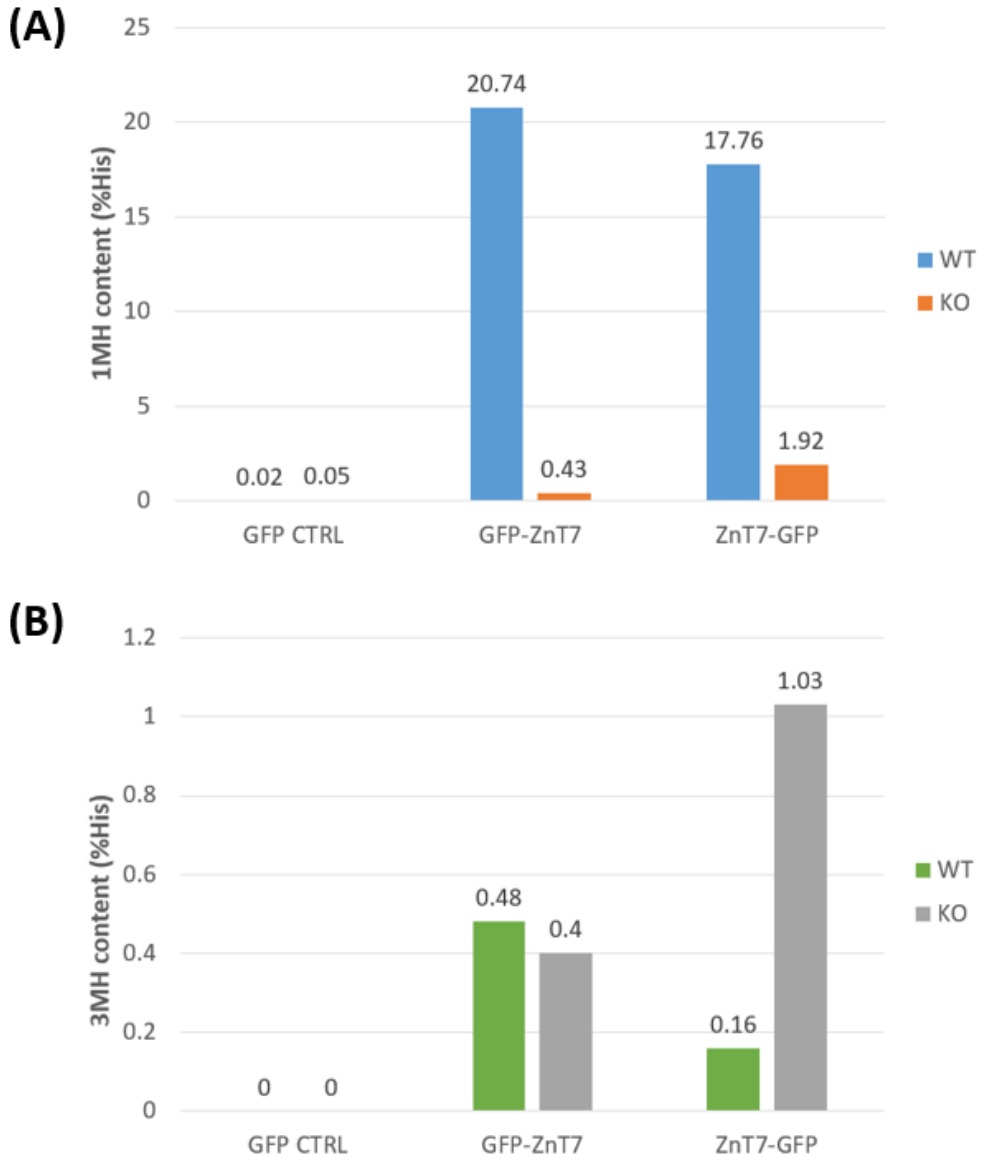

Figure 24: Methyl histidine content in GFP-tagged ZnT7 proteins transiently expressed in WT and METTL9 KO HEK293T cells. Graph displayed in (A) demonstrates the difference in 1MH content (in % of unmodified histidine) between WT (blue) and METTL9 KO (orange) HEK293T cells, whereas

the graph displayed in (B) demonstrates the difference in 3MH content (in % of unmodified histidine) between WT (green) and METTL9 KO (grey) HEK293T cells.

Figure 24 (A) displays the 1MH content in the two GFP-tagged ZnT7 proteins, and it is clear that the amount of 1MH is much greater in samples immunoprecipitated from WT HEK293T cells compared to the METTL9 KO HEK293T cells. As demonstrated by the blue bar in Figure 24 (A), there appears to be around 20% 1MH compared to unmethylated histidine for both GFP-ZnT7 and ZnT7-GFP. In the samples immunoprecipitated from METTL9 KO HEK293T cells (orange bar, Figure 24 (A)), there appears to be around 0.4% and 2% 1MH compared to unmodified histidine for GFP-ZnT7 and ZnT7-GFP respectively. As the 1MH content is significantly decreased when METTL9 is not present (in the METTL9 KO cells, orange bar in Figure 24 (A)), this demonstrates that METTL9 does in fact methylate ZnT7 *in vivo* in HEK293T cells.

Figure 24 (B) shows the 3MH content in samples from both WT and METTL9 KO HEK293T cells. We expected minimal differences in 3MH content of GFP-tagged ZnT7 isolated from WT and METTL9 KO cells. There should be little contamination from other proteins, as the proteins had been immunoprecipitated prior to the amino acid hydrolysis (AAH) and the following AAA. As METTL9 is a 1MH-specific MTase [42], and thus does not yield 3MH there should here be a minimal difference in regard to whether METTL9 is present (WT, green bar in Figure 24 (B)) or not (KO, grey bar in Figure 24 (B)). This seems indeed to be the case for GFP-ZnT7, however for ZnT7-GFP, the amount of 3MH is much higher in the sample isolated from the KO cells. For the GFP control, the amount of 3MH was zero for both WT and METTL9 KO samples.

4. Discussion

4.1 Confirmation of expression and localization of ZnT5 and ZnT7

4.1.1 Stable transfections of WT HeLa and WT HAP1 cells

Attempts to create WT HeLa and WT HAP1 cell lines stably expressing GFP-tagged ZnT5 and ZnT7 proved futile, as no expression of these proteins could be observed either in a pool (Figure 13 (A)) or several colonies (Figure 14 (A)) of cells surviving selection with G418/Geneticin. This was surprising since at least the WT HeLa (but not WT HAP1) cells appeared to be transfected efficiently, as was observed with the ZOE Imager a day post transfection (Figure 12 (B)) and multiple colonies formed after some weeks following selection with G418/Geneticin (results not shown). However, after selection with G418/Geneticin, we no longer saw any GFP signal from the GFP-tag in the surviving cells using the Zoe Imager (results of this are not shown). This could be due to complete absence or a low level of expression of the GFP-tagged zinc transporters. We did see expression of the GFP-only control after selection, but GFP is expressed throughout the cell, whereas the subcellular localization of ZnT5 and ZnT7 is not reported to be ubiquitous, but rather localized to a much smaller part of the cell, such as the Golgi [53, 60, 63]. This means that the signals emitted from the GFP-tag expressed by the zinc transporter proteins would be correspondingly weaker than the expression of the GFP-only control. Thus, the fact that we did not observe any GFP signal after selection with G418/Geneticin does not mean that the GFP-tagged zinc transporters had not been transfected efficiently, but rather that their expression could have been low (or absent) in combination with a weaker GFP signal.

Why the stable transfection of WT HeLa and WT HAP1 cells was unsuccessful even though there were observed resistant colonies can be due to a number of reasons. During the initial experiments an expired secondary antibody was used which could explain why this antibody appeared very un-specific and thus yielding a high degree of background “noise” as can be observed in Figures 13 and 14 (A). When it was eventually discovered that this antibody was rather old, a new secondary antibody was used for the analysis of lysates from transiently transfected WT and METTL9 KO HEK293T cells, results of which can be seen in Figure 17 (A). Thus, the issue of not observing any protein expression in lysates from the WT HeLa and WT HAP1 cell lines could be technical.

Another reason could be that as stable transfection entails that the plasmid (pEGFPC1 and pEGFPN1) is integrated into a random genomic locus, it could be that the plasmid was integrated into a genomic region with low levels of gene expression, and thus just enough gene

expression occurred to express the G418/Geneticin resistance gene, which would enable the cells to survive, but not enough gene expression to produce any visible amounts of ZnT5 or ZnT7. In addition, if larger amounts of these proteins are toxic to the cells, the cells would preferably overexpress GFP-tagged ZnTs in small amounts (or none at all) in order to survive, and thus their expression could be affected in this way as well [75].

ZnT5 and ZnT7 are transmembrane proteins, and the usual lysis methods using RIPA as a lysis buffer are in some cases inefficient for membrane proteins. Transmembrane proteins are very hydrophobic and tend to aggregate and thus might get lost in the pellet during the lysis process with RIPA. RIPA contains a low amount of detergent, whereas LDS, for example, contains a very high amount which is why LDS is mostly used to denature proteins. In this way RIPA simply solubizes cell membranes whilst LDS does both. If the WT HeLa and WT HAP1 cells had been lysed with LDS directly, some signal for GFP-tagged ZnT5 and ZnT7 might have been observed on the WB (Figure 13 (A)). However, for further experiments, such as fluorography to assess methylation activity on the zinc transporter proteins, this would have required the proteins in their non-denatured state, thus using LDS to prepare lysates could only have been done in order to confirm protein expression.

4.1.2 Transient transfection of WT and METTL9 KO HEK293T cells

Performing transient transfections, where the genes of interest are not integrated into the genome, proved to work better for the purpose of this study. In particular for the confirmed expression of both C- and N-terminally tagged ZnT7, as can be seen in Figure 17, (A). Expression of GFP-tagged ZnT5 was never confirmed via WB, although the GFP-tagged protein was observed ~24 hours post-transfection in both WT and METTL9 KO HEK293T cells when looking at cells using the ZOE Imager. It could be that what was observed in both ZOE Imager pictures of GFP-tagged ZnT5 (Figure 15) and using the Olympus FluoView microscope (Figure 19) is an artifact of some sort, but as the protein localized to regions supported by previous reports [63], the problem most likely lies with the WB. As mentioned previously, transmembrane proteins, such as zinc transporters tend to aggregate and thus might get lost in the pellet during the lysis process with RIPA buffer. For transiently transfected HEK293T WT and METTL9 KO cells it was attempted to lyse the cells using NuPAGE® LDS sample buffer (4x) (Invitrogen), though this did not yield high protein concentrations and results of this are not shown. As mentioned in the introduction, ZnTs usually contain a total of 6 TMDs, but ZnT5 contains an additional 9 for a total of 15 TMDs [64] which could be why this protein was difficult to verify expression of.

Nonetheless, subsequent experiments were performed using WT and METTL9 KO HEK293T cells transiently transfected with GFP-tagged ZnT5 and ZnT7. As the genes expressed by the constructed plasmid are gradually lost during growth and cell division when performing transient transfections, the WT and METTL9 KO HEK293T cells had to be re-transfected with the constructed plasmid (GFP-tagged ZnT5 and ZnT7) for various experiments once frozen sample lysate was running low. For this reason, creating a stably transfected cell line expressing ZnT5 and ZnT7 would have been preferred as having to continuously re-transfect is rather unfavorable and time consuming. Therefore, one limitation of our methods was the plasmids we used, pEGFPC1 and pEGFPN1 with the selectable marker for neomycin/geneticin resistance, which HEK293T are already resistant to. If there had been enough time, we should have re-cloned the GFP-tagged genes into another plasmid, with a different selection maker. In this way we could have performed stable transfections using WT and METTL9 KO HEK293T cells.

4.1.3 Localization studies via microscopy

Using transiently transfected WT and METTL9 KO HEK293T cells expressing ZnT5 and ZnT7, localization of said zinc transporters was observed using an Olympus FluoView microscope. Due to various time constraints, localization was only observed and studied for C-terminally tagged ZnT5 and ZnT7.

No big differences were observed in the localization pattern of ZnT5 and ZnT7 regarding the presence or absence of METTL9 as can be seen in Figure 18 (C-terminally tagged ZnT7) and 19 (C-terminally tagged ZnT5). C-terminally tagged ZnT5 and ZnT7 were observed to primarily localize to regions reminiscent of the early secretory pathway, which is consistent with previous reports for both proteins [53, 60, 63, 76]. The C-terminal GFP-tag did not seem to interfere with the localization of ZnT5 or ZnT7, since observed localization is as expected.

Observed localization pattern of both GFP-tagged ZnT5 and ZnT7 appeared to be independent upon the presence of METTL9 in the cells, when comparing protein localization in WT versus METTL9 KO HEK293T cells. For ZnT7, which we later confirmed by AAA to be methylated in the WT HEK293T cells, as can be noted from Figure 24, this would imply that methylation of this zinc transporter does not alter its final location in the growth conditions studied in this thesis. ZnT7 has been shown to localize to the Golgi, specifically the Golgi membrane [60, 76], so these findings do align with the previously reported localization of ZnT7. Note that in a study performed by Gao et. al [76], endogenous, and not overexpressed, ZnT7 in mice have been used to study localization using specific anti-ZnT7 antibodies. In addition, in a study by Tuncay et.al from 2017 [62], ZnT7 was also found to localize to the ER in heart muscle cells, and as

can be noted from Figure 20, there might have been some overlap between ZnT7-GFP and the ER (as indicated by the yellow regions), but this could also display contact sites between the ER and the Golgi.

Human ZnT5 has two different splice variants and in previous studies the canonical isoform of ZnT5, variant A, has been shown to localize to the Golgi apparatus [59, 63] while variant B has been observed to localize to the ER [63]. These two variants differ in their C-terminal region, as a result from the incorporation into the mature transcript of either the whole of exon 14 (yielding variant B which is retained in the ER) or only the 5' region of exon 14 plus exons 15-17 (variant A which is trafficked to the Golgi) [63]. In the experiments described in this thesis ZnT5 (the canonical isoform, variant A) was only observed to display a speckled distribution around the nucleus, which is likely the Golgi apparatus, but as the expression of ZnT5 in HEK293T WT and METTL9 KO cells was never confirmed via WB (Figures 13 and 14 (A) as well as Figure 17 (A)), the results of this experiment are not 100% conclusive and there is a need for further corroboration. In addition, it would be interesting to study the localization of variant B of ZnT5, both C- and N-terminally tagged, in WT and METTL9 KO cells.

4.2 *In vitro* methylation of ZnT7 by METTL9

After confirming protein expression of ZnT7 (Figure 17), both C-terminally and N-terminally tagged, GST-hsMETTL9 was purified for a subsequent MTase assay to assess the enzyme's activity on both ZnT5 and ZnT7. The results of said MTase assay can be observed on the fluorography film shown in Figure 22 (A). As ZnT5 expression could not be verified via WB, we hoped that perhaps the methylation signal would be stronger than the antibody signal (on the WB, Figure 17). Thus, if the issue with the WB was that the signal was too weak, we could have perhaps observed ZnT5 on the fluorography film and therefore ZnT5 was included in the MTase assay.

When performing a METTL9 MTase assay using mammalian cell extracts as substrates, two substrates are usually visible on the fluorography film, one of which is around 45 kDa and the other around 30 kDa [42]. The identity of the proteins in these bands is so far not known [42]. When looking at the fluorography film shown in Figure 22 (A), these yet-unknown substrates appear to be present in all cell lysates containing GFP-tagged ZnT5. These bands are, however, rather weak, possibly due to poor enzyme quality. When GST-hsMETTL9 was purified, the elution buffer (Appendix) used to collect final GST-hsMETTL9 eluate was not mixed properly and the glutathione was not properly dissolved in the initial steps of the elution (for proper protocol see section 2.6.1, Materials and Methods). This would have led to a low concentration of glutathione initially and a lot of protein would then be left on the column, and

thus not be eluted. However, the fact that these two typical METTL9 substrates can be observed on the fluorography film, see Figure 22 (A), for the ZnT5 samples, and also that these bands appear to be stronger in samples collected from KO cells compared to WT cells, indicate that the assay has worked as expected and that the correct lysate has been used.

For all the samples containing GFP-tagged ZnT7 the story is somewhat different. Here there appears to be no methylation of these two known METTL9 targets (Figure 22 (A)). The only methylated product appears to be GFP-tagged ZnT7, although the band is also here rather weak, but around expected size, see Figure 22 (A) along with figure legend. Whilst loading samples onto the SDS-PAGE gel, there was some overflow from the well containing METTL9 KO ZnT7-GFP into the lane containing the GFP-control (from WT HEK293T cells). Surprisingly, ZnT7 from WT HEK293T cells appeared to be more strongly methylated *in vitro* by METTL9 as compared to ZnT7 from the METTL9 KO HEK293T cells. We would expect the opposite, as in WT cells the protein would already be (at least partially) methylated by METTL9, which we also confirmed by the AAA (see Figure 24 (A)). Lysates containing ZnT7 did have a somewhat lower protein concentration compared to lysates containing ZnT5, but they were rather similar to each other, with even more material in the lysates from METTL9 KO HEK293T cells. A WB could be performed on the stained membrane from Figure 22 (B) to compare the amount of GFP-tagged protein levels from WT and METTL9 KO samples, which may explain why methylation of GFP-tagged ZnT7 from WT cells appears stronger. Do to time constraints this was not done.

4.3 *In vivo* methylation of ZnT7

As the MTase assay revealed no observed in vitro methylation by METTL9 by fluorography for samples containing GFP-tagged ZnT5 (see Figure 22 (A)), only GFP-tagged ZnT7 was used for further analysis. ZnT7 tagged with GFP on either terminus was immunoprecipitated by GFP-trap using lysates of WT and METTL9 KO HEK293T cells expressing the corresponding constructs. Samples were run on an SDS-PAGE and appropriate bands containing the GFP-tagged ZnT7 were cut out from said gel and hydrolyzed. WB membrane and corresponding gel is depicted in Figure 23. The AAA of the samples showed that the amount of 1MH was about five-fold higher in the ZnT7 samples immunoprecipitated from WT HEK293T cells compared to the samples from the METTL9 KO HEK293T cells (see Figure 24 (A)).

These results indicate that ZnT7 is methylated *in vivo*, and this methylation is generated by METTL9, as the 1MH content is decreased (to almost background levels) in the METTL9 KO cells. As this analysis was done utilizing both C- and N-terminally tagged ZnT7, this is in a way a duplicate and thus a robust result. Minimal amounts of 3MH were observed in all samples

(apart from background levels) which is to be expected, as METTL9 is 1MH-specific and no 3MH-specific MTases are known to specifically target the ZnTs. The fact that some 3MH still could be read from the samples (see Figure 24 (B)), could perhaps indicate co-precipitation of actin (or another 3MH-containing protein), or it could be inaccuracy of the instrument used for measuring. The GFP-control shows near null amounts of both 1MH and 3MH content which was also as expected.

In Figure 24 ZnT7-GFP has somewhat higher levels of 1MH and 3MH in samples taken from METTL9 KO cells. The reason for this is not known, but this could be a technical issue either with the instrument at NTNU used for measuring or with the loading of the samples on the SDS-PAGE gel, prior to performing the AAH on extracted gel-pieces. The immunoprecipitated samples should defiantly have been sonicated prior to being loaded on the gel, as possible DNA contamination made the samples sticky and difficult to load. In addition, there could have been some carry-over as no lanes were skipped in-between samples, although samples from WT and samples from METTL9 KO HEK293T cells were loaded pretty far apart (see Figure 23).

4.4 Proposed functions of his-rich region in zinc transporter proteins

As mentioned in the introduction of this thesis, one of the reasons why zinc transporter proteins make for interesting possible substrates of METTL9 is their high number of HxH-motifs, which is preferred by METTL9 for 1MH modifications. These HxH-motifs are found in a cytosolic his-rich region in most zinc transporter proteins. A demonstration of what this his-rich region looks like in the AlphaFold predicted structure of ZnT5 and ZnT7 is shown in Figure 25.

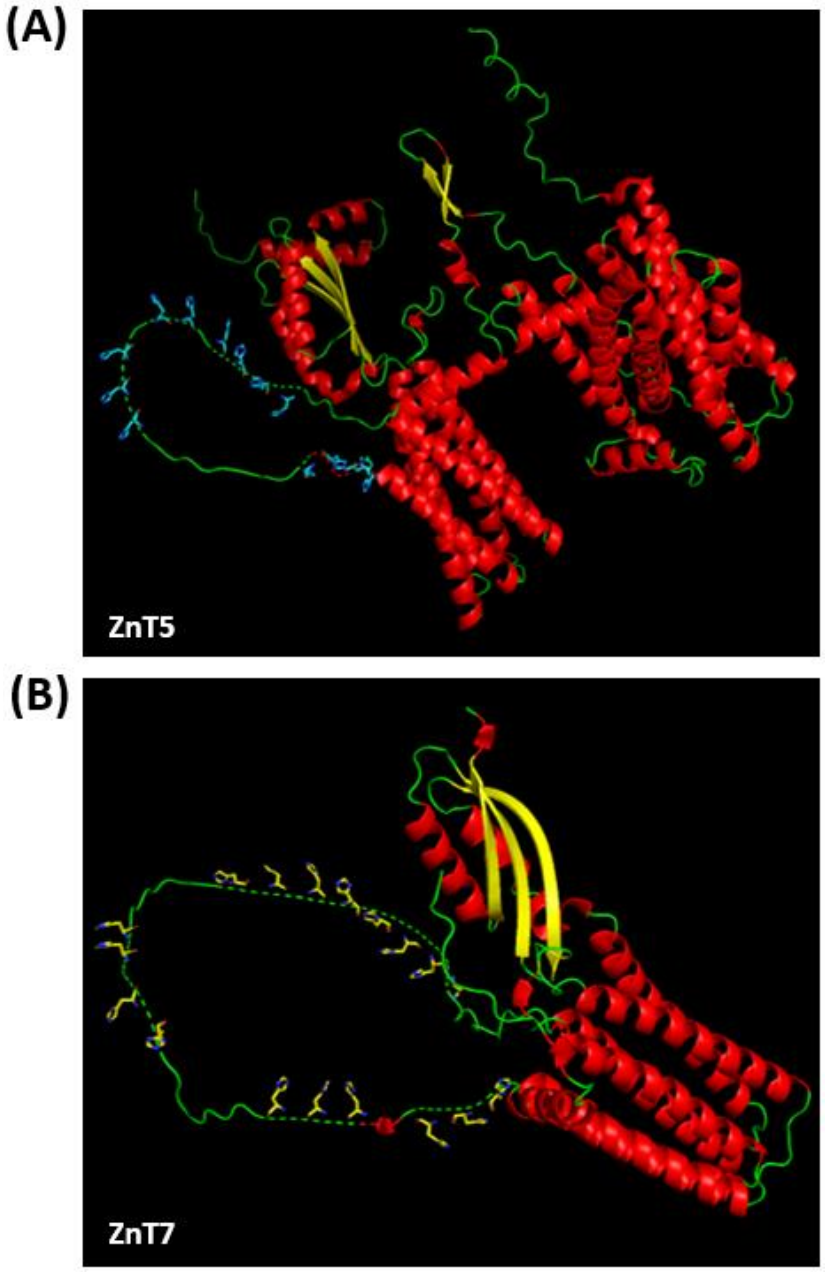

Figure 25: AlphaFold predicted structure of ZnT5 (A) and ZnT7 (B). Figure generated by downloading AlphaFold predicted structure (UniProt KB) and rendering it in PyMOL (Version 4.6.0). α-helices are shown in red, loops and unstructured regions are shown in green and β-sheets are shown in yellow. Histidine residues in the histidine-rich region are shown as sticks and colored in blue for ZnT5 (A) and yellow for ZnT7 (B).

The function of this region is still a topic of debate, but proposed theories include that it is important for zinc binding and transport. In a study by Fukue et.al from 2018 [55] both the his-rich region and the unique N-terminus possessed by most zinc transporter proteins was investigated. In this study the authors conclude that the histidine residues of the hist-rich region were not essential for zinc transport by ZnTs, but that they possibly participate in modulating zinc transport activity. They also suggest that the N-terminal region might interact with the histidine-rich region and that they together modulate zinc transport.

Another theory is that this region is in part responsible for the metal selectivity of most zinc transporter proteins and serves as a possible zinc sensor. Zinc transporter proteins are highly sensitive to zinc and have been seen to discriminate between zinc ions (Zn^{2+}) and other metal ions such as cadmium ions (Cd^{2+}) [77]. It has therefore been suggested that the his-rich region in most ZnTs is responsible for this metal selectivity.
However, in a study by Hoch et.al in 2012 [77] it was discovered that the discrimination between these two metal ions is reliant on specific residues in the transport site (the binding site of Zn^{2+}), thus a site unrelated to this region dense in histidine residues. As histidine residues as frequently used by proteins to coordinate metals, the authors further speculate whether this histidine-rich region perhaps serve to increase the metal concentration above the threshold for selective transport and thus are indirectly involved in the selective binding of zinc over other metal cations. The authors also note that various plant ZnT7 homologous are less selective and transport other metals [77]. Why there is a difference in selectivity between plant and mammalian ZnT homologous is not known, but the authors speculate that the his-rich region is part of it. As (land) plants are not known to express METTL9 [42], it might be that this more stringent metal selectivity in mammals could be due to methylation of the his-rich region by METTL9, and that upon methylation the metal concentration is not increased above the threshold for selective transport and thus affinity for zinc, and further selectivity, is decreased.

The expression of zinc transporters is controlled by the concentration of zinc present in their cellular environment [78] but otherwise their regulation is rather elusive. Thus, this region, and the methylation of parts of this region by METTL9, could be vital in terms of zinc transport activity. In the study by Davydova et.al [42], zinc transport in the cell was not evaluated, but when they investigated a methylated peptide from a his-rich region of ZIP7, this peptide had a lower affinity for zinc than when this region was unmethylated. For the immunomodulatory protein S100A9, something similar was observed with zinc binding being significantly reduced upon methylation mediated by METTL9 [44]. Thus, this region, and its methylation mediated by METTL9, might be vital in terms of zinc affinity, which in turn is relevant for zinc transporter activity. Lower affinity for zinc does not mean lower affinity for other metals, at least in the case of S100A9 which also coordinates other metal cations such as cadmium. But for zinc transporters which show a high degree of selectivity, a lowered zinc affinity could also have an impact on activity. Thus, investigation into METTL9 mediated methylation of this region in a variety of zinc transporters, could help in determining A) the function of the histidine-rich region, and B) how zinc transporters are regulated.

The consensus for the function of this histidine-rich region is that it has relevance for the metal transport provided by zinc transporters. The fact that when this region is methylated in a ZIP7-derived peptide, its affinity for zinc decreases, demonstrates this. However, whether this decreased affinity is due to a change in selectivity or decreased transport activity is not known. Decreased affinity for zinc could perhaps just mean that the zinc transporter loses its selectivity and thus does not discriminate between other metals as well as when unmethylated. Given the mentioned proposed function of the histidine-rich region and the fact that METTL9 is responsible for its methylation, at least in zinc transporters, we can speculate that methylation regulates this regions function in one way or another. 1MH content has never been taken into consideration when determining the function of this conserved region in zinc transporters, and it is therefore very likely that elucidating the function of METTL9 mediated methylation will help cast a light on the function of this region as well.

5. Conclusion and future perspectives

From work presented in this thesis, several conclusions can be drawn. Firstly, localization of GFP-tagged ZnT5 and ZnT7 did not seem to be affected by the absence of METTL9 in HEK293T cells. However, there is a need for duplicate experiments with WT and METTL9 KO HEK293T cells as during imaging very few cells were looked at as the transfection efficiency was not optimal. Thus, redoing the experiment with a higher transfection efficiency and observing more cells under the microscope would be of interest. It would also be pivotal to use different stains as in perhaps stains for Golgi and/or vesicles instead of ER, to better observe from which compartments within the cell the GFP-signal originates. As previously mentioned, there was some overlap with the ER-stain for METTL9 KO HEK293T cells transiently transfected with ZnT7-GFP and re-doing this experiment with re-transfected cells and a better ER-tracker should be performed to elucidate this. In addition, N-terminally tagged ZnT5 and ZnT7 and their localization pattern in the presence or absence of METTL9 needs further corroboration as their localization was not studied in experiments performed in this thesis. Multiple membrane proteins localized to the secretory pathway, have been identified as having or are predicted to have an N-terminal signal peptide targeting them to the ER and subsequently to their final locations [79, 80]. Such a signal peptide would have the potential of being blocked by the addition of an N-terminal GFP-tag. As zinc transporters are transmembrane proteins, the majority of them are predicted by UniProt KB to carry such a tag, but to date, no such tag is listed as predicted for ZnT5 or ZnT7. We did not investigate localization of N-terminally tagged ZnT5 and ZnT7 by microscopy, but this would be something to do in the future. However, we did observe robust expression of N-terminally tagged ZnT7 in the WB (Figure 17), the MTase assay (Figure 22) and the AAA (Figure 24), which likely would not be the case if a vital N-terminal signal peptide was disturbed.

The second conclusion that can be drawn from this study is that the zinc transporter ZnT7 can be *in vitro* methylated by METTL9 as a full protein. In the past activity has only been shown on a short peptide [42]. Finally, we conclusively show that GFP-tagged ZnT7 indeed contains 1MH modifications when transiently overexpressed in WT HEK293T cells, as displayed by the AAA, which can be found in Figure 24. There was a notable decrease in the amount of 1MH content in the METTL9 KO HEK293T derived samples, compared to the WT samples, which supports the incorporation of 1MH in ZnT7 by METTL9. As both N-terminally and C-terminally tagged ZnT7 was verified as having a high 1MH content in WT but not METTL9 KO cells, this result is robust as this is a duplicate of the same protein only with GFP-tags on different protein ends. However, experiments should be repeated to confirm both the presence of 1MH in ZnT7 as well as the percentage of methylation in the full-length protein, and an MS analysis of the

full-length human ZnT7 protein would also be of interest in order to investigate methylation sites utilized by METTL9.

The approach of transient overexpression of GFP-tagged proteins in WT and METTL9 KO HEK293T cells, followed by IP and AAA, could in the future be applied to other zinc transporters to confirm whether they are indeed *in vivo* METTL9 substrates. It would also be interesting to perform these experiments in different cell growth conditions, such as high- or low-metal concentrations in the growth medium, to see how this would affect METTL9-mediated methylation of these transporters. Additionally, measuring the activity of ALPs, whose activation by zinc-loading is dependent on ZnT5-ZnT7 as mentioned in the introduction, would be of interest as ZnT5 and ZnT7 are possibly regulated by METTL9. If one were to culture WT and METTL9 KO cells in low zinc conditions, as low zinc conditions would make the effect stronger, activity of the ALPs should be effected if activity of the ZnTs are affected.

Bibliography

1. Keskin, O., et al., *Principles of Protein–Protein Interactions: What are the Preferred Ways For Proteins To Interact?* Chemical Reviews, 2008. **108**(4): p. 1225-1244.
2. Nilsen, T.W. and B.R. Graveley, *Expansion of the eukaryotic proteome by alternative splicing.* Nature, 2010. **463**(7280): p. 457-463.
3. Bagwan, N., H.H. El Ali, and A. Lundby, *Proteome-wide profiling and mapping of post translational modifications in human hearts.* Scientific Reports, 2021. **11**(1): p. 2184.
4. Uversky, V.N., *Posttranslational Modification*, in *Brenner's Encyclopedia of Genetics (Second Edition)*, S. Maloy and K. Hughes, Editors. 2013, Academic Press: San Diego. p. 425-430.
5. Ramazi, S. and J. Zahiri, *Post-translational modifications in proteins: resources, tools and prediction methods.* Database, 2021. **2021**.
6. Cheng, X. and R.J. Roberts, *AdoMet-dependent methylation, DNA methyltransferases and base flipping.* Nucleic Acids Research, 2001. **29**(18): p. 3784-3795.
7. Fontecave, M.A., Mohamed and E. Mulliez, *S-adenosylmethionine: Nothing goes to waste.* Trends in Biochemical Sciences 2004. **29**(5): p. 243-249.
8. Petrossian, T.C. and S.G. Clarke, *Uncovering the Human Methyltransferasome *.* Molecular & Cellular Proteomics, 2011. **10**(1).
9. Lennard, L., *4.21 - Methyltransferases*, in *Comprehensive Toxicology (Second Edition)*, C.A. McQueen, Editor. 2010, Elsevier: Oxford. p. 435-457.
10. Schubert, H.L., R.M. Blumenthal, and X. Cheng, *Many paths to methyltransfer: a chronicle of convergence.* Trends in Biochemical Sciences, 2003. **28**(6): p. 329-335.
11. Falnes, Pål Ø., et al., *Protein lysine methylation by seven-β-strand methyltransferases.* Biochemical Journal, 2016. **473**(14): p. 1995-2009.
12. Dillon, S.C., et al., *The SET-domain protein superfamily: protein lysine methyltransferases.* Genome Biology, 2005. **6**(8): p. 227.
13. Małecki, J.M., et al., *Human METTL18 is a histidine-specific methyltransferase that targets RPL3 and affects ribosome biogenesis and function.* Nucleic Acids Res, 2021. **49**(6): p. 3185-3203.
14. Ragsdale, S.W., *Catalysis of Methyl Group Transfers Involving Tetrahydrofolate and B12*, in *Vitamins & Hormones*. 2008, Academic Press. p. 293-324.
15. Raju, T.S., *Methylation of Proteins*, in *Co- and Post-Translational Modifications of Therapeutic Antibodies and Proteins*. 2019. p. 133-146.
16. Małecki, J.M., E. Davydova, and P.Ø. Falnes, *Protein methylation in mitochondria.* Journal of Biological Chemistry, 2022. **298**(4): p. 101791.
17. Biggar, K.K. and S.S.C. Li, *Non-histone protein methylation as a regulator of cellular signalling and function.* Nature Reviews Molecular Cell Biology, 2015. **16**(1): p. 5-17.
18. Jakobsson, M.E., *Enzymology and significance of protein histidine methylation.* Journal of Biological Chemistry, 2021. **297**(4).
19. Kouzarides, T., *Histone methylation in transcriptional control.* Current Opinion in Genetics & Development, 2002. **12**(2): p. 198-209.
20. Shi, Y., et al., *Histone Demethylation Mediated by the Nuclear Amine Oxidase Homolog LSD1.* Cell, 2004. **119**(7): p. 941-953.
21. Greer, E.L. and Y. Shi, *Histone methylation: a dynamic mark in health, disease and inheritance.* Nature Reviews Genetics, 2012. **13**(5): p. 343-357.

22. Tsukada, Y.-i., et al., *Histone demethylation by a family of JmjC domain-containing proteins.* Nature, 2006. **439**(7078): p. 811-816.
23. Walport, L.J., et al., *Arginine demethylation is catalysed by a subset of JmjC histone lysine demethylases.* Nature Communications, 2016. **7**(1): p. 11974.
24. Chang, B., et al., *JMJD6 Is a Histone Arginine Demethylase.* Science, 2007. **318**(5849): p. 444-447.
25. Jambhekar, A., A. Dhall, and Y. Shi, *Roles and regulation of histone methylation in animal development.* Nature Reviews Molecular Cell Biology, 2019. **20**(10): p. 625-641.
26. Clarke, S.G., *Protein methylation at the surface and buried deep: thinking outside the histone box.* Trends Biochem Sci, 2013. **38**(5): p. 243-52.
27. Dhayalan, A. and A. Jeltsch, *Special Issue "Structure, Activity, and Function of Protein Methyltransferases".* Life (Basel), 2022. **12**(3).
28. Di Blasi, R., et al., *Non-Histone Protein Methylation: Biological Significance and Bioengineering Potential.* ACS Chemical Biology, 2021. **16**(2): p. 238-250.
29. Hwang, J.W., et al., *Protein arginine methyltransferases: promising targets for cancer therapy.* Experimental & Molecular Medicine, 2021. **53**(5): p. 788-808.
30. Zhao, S., C.D. Allis, and G.G. Wang, *The language of chromatin modification in human cancers.* Nature Reviews Cancer, 2021. **21**(7): p. 413-430.
31. Asatoor, A.M. and M.D. Armstrong, *3-Methylhistidine, a component of actin.* Biochemical and Biophysical Research Communications, 1967. **26**(2): p. 168-174.
32. Johnson, P., C.I. Harris, and S.V. Perry, *3-methylhistidine in actin and other muscle proteins.* Biochem J, 1967. **105**(1): p. 361-70.
33. Huszar, G. and M. Elzinga, *Homologous Methylated and Nonmethylated Histidine Peptides in Skeletal and Cardiac Myosins.* Journal of Biological Chemistry, 1972. **247**(3): p. 745-753.
34. Liao, S.M., et al., *The multiple roles of histidine in protein interactions.* Chem Cent J, 2013. **7**(1): p. 44.
35. Zhu, R., et al., *Allosteric histidine switch for regulation of intracellular zinc(II) fluctuation.* Proceedings of the National Academy of Sciences, 2017. **114**(52): p. 13661-13666.
36. Kapell, S. and M.E. Jakobsson, *Large-scale identification of protein histidine methylation in human cells.* NAR Genomics and Bioinformatics, 2021. **3**(2).
37. Kwiatkowski, S., et al., *SETD3 protein is the actin-specific histidine N-methyltransferase.* Elife, 2018. **7**.
38. Wilkinson, A.W., et al., *SETD3 is an actin histidine methyltransferase that prevents primary dystocia.* Nature, 2019. **565**(7739): p. 372-376.
39. Webb, K.J., et al., *A Novel 3-Methylhistidine Modification of Yeast Ribosomal Protein Rpl3 Is Dependent upon the YIL110W Methyltransferase* Journal of Biological Chemistry, 2010. **285**(48): p. 37598-37606.
40. Cloutier, P., et al., *A Newly Uncovered Group of Distantly Related Lysine Methyltransferases Preferentially Interact with Molecular Chaperones to Regulate Their Activity.* PLOS Genetics, 2013. **9**(1): p. e1003210.
41. Holm, M., et al., *Differences and overlap in plasma protein expression during colorectal cancer progression.* Translational Medicine Communications, 2019. **4**(1): p. 14.
42. Davydova, E., et al., *The methyltransferase METTL9 mediates pervasive 1-methylhistidine modification in mammalian proteomes.* Nature Communications, 2021. **12**(1): p. 891.

43. Lv, M., et al., *METTL9 mediated N1-histidine methylation of zinc transporters is required for tumor growth.* Protein Cell, 2021. **12**(12): p. 965-970.
44. Daitoku, H., et al., *siRNA screening identifies METTL9 as a histidine Nπ-methyltransferase that targets the proinflammatory protein S100A9.* J Biol Chem, 2021. **297**(5): p. 101230.
45. Foster, K.J., et al., *Retinoic acid receptor beta variant-related colonic hypoganglionosis.* American Journal of Medical Genetics Part A, 2019. **179**(5): p. 817-821.
46. Sugiyama, K., et al., *Mid-Frequency Hearing Loss Is Characteristic Clinical Feature of OTOA-Associated Hearing Loss.* Genes, 2019. **10**(9): p. 715.
47. RAFTERY, M.J., et al., *Isolation of the murine S100 protein MRP14 (14 kDa migration-inhibitory-factor-related protein) from activated spleen cells: characterization of post-translational modifications and zinc binding.* Biochemical Journal, 1996. **316**(1): p. 285-293.
48. Chen, P.H., et al., *Zinc transporter ZIP7 is a novel determinant of ferroptosis.* Cell Death Dis, 2021. **12**(2): p. 198.
49. Sapkota, M. and D.L. Knoell, *Essential Role of Zinc and Zinc Transporters in Myeloid Cell Function and Host Defense against Infection.* J Immunol Res, 2018. **2018**: p. 4315140.
50. Hara, T., et al., *Zinc transporters as potential therapeutic targets: An updated review.* Journal of Pharmacological Sciences, 2022. **148**(2): p. 221-228.
51. Suzuki, T., et al., *Zinc Transporters, ZnT5 and ZnT7, Are Required for the Activation of Alkaline Phosphatases, Zinc-requiring Enzymes That Are Glycosylphosphatidylinositol-anchored to the Cytoplasmic Membrane *.* Journal of Biological Chemistry, 2005. **280**(1): p. 637-643.
52. Chimienti, F., et al., *Zinc Homeostasis-regulating Proteins: New Drug Targets for Triggering Cell Fate.* Current Drug Targets, 2003. **4**(4): p. 323-338.
53. Kambe, T., E. Suzuki, and T. Komori, *Zinc Transporter Proteins: A Review and a New View from Biochemistry*, in *Zinc Signaling*, T. Fukada and T. Kambe, Editors. 2019, Springer Singapore: Singapore. p. 23-56.
54. Norouzi, S., et al., *Zinc transporters and insulin resistance: therapeutic implications for type 2 diabetes and metabolic disease.* Journal of Biomedical Science, 2017. **24**(1): p. 87.
55. Fukue, K., et al., *Evaluation of the roles of the cytosolic N-terminus and His-rich loop of ZNT proteins using ZNT2 and ZNT3 chimeric mutants.* Scientific Reports, 2018. **8**(1): p. 14084.
56. Chang, C. and Z. Werb, *The many faces of metalloproteases: cell growth, invasion, angiogenesis and metastasis.* Trends Cell Biol, 2001. **11**(11): p. S37-43.
57. Wong, M.K.-S., *Subchapter 42D - Angiotensin converting enzyme*, in *Handbook of Hormones (Second Edition)*, H. Ando, K. Ukena, and S. Nagata, Editors. 2021, Academic Press: San Diego. p. 505-508.
58. Fedde, K.N., et al., *Alkaline Phosphatase Knock-Out Mice Recapitulate the Metabolic and Skeletal Defects of Infantile Hypophosphatasia.* Journal of Bone and Mineral Research, 1999. **14**(12): p. 2015-2026.
59. Kambe, T., et al., *Cloning and Characterization of a Novel Mammalian Zinc Transporter, Zinc Transporter 5, Abundantly Expressed in Pancreatic β Cells *.* Journal of Biological Chemistry, 2002. **277**(21): p. 19049-19055.
60. Kirschke, C.P. and L. Huang, *ZnT7, a Novel Mammalian Zinc Transporter, Accumulates Zinc in the Golgi Apparatus *.* Journal of Biological Chemistry, 2003. **278**(6): p. 4096-4102.
61. KAMBE, T., *An Overview of a Wide Range of Functions of ZnT and Zip Zinc Transporters in the Secretory Pathway.* Bioscience, Biotechnology, and Biochemistry, 2011. **75**(6): p. 1036-1043.

62. Tuncay, E., et al., *Hyperglycemia-Induced Changes in ZIP7 and ZnT7 Expression Cause Zn2+ Release From the Sarco(endo)plasmic Reticulum and Mediate ER Stress in the Heart.* Diabetes, 2017. **66**(5): p. 1346-1358.
63. Thornton, J.K., et al., *Differential subcellular localization of the splice variants of the zinc transporter ZnT5 is dictated by the different C-terminal regions.* PLoS One, 2011. **6**(8): p. e23878.
64. Kambe, T., et al., *Overview of mammalian zinc transporters.* Cellular and Molecular Life Sciences CMLS, 2004. **61**(1): p. 49-68.
65. Fukunaka, A., et al., *Demonstration and Characterization of the Heterodimerization of ZnT5 and ZnT6 in the Early Secretory Pathway *.* Journal of Biological Chemistry, 2009. **284**(45): p. 30798-30806.
66. Wagatsuma, T., et al., *Zinc transport via ZNT5-6 and ZNT7 is critical for cell surface glycosylphosphatidylinositol-anchored protein expression.* J Biol Chem, 2022. **298**(6): p. 102011.
67. Huang, L., et al., *Znt7 (Slc30a7)-deficient Mice Display Reduced Body Zinc Status and Body Fat Accumulation *.* Journal of Biological Chemistry, 2007. **282**(51): p. 37053-37063.
68. Kable, M.E., et al., *The Znt7-null mutation has sex dependent effects on the gut microbiota and goblet cell population in the mouse colon.* PLOS ONE, 2020. **15**(9): p. e0239681.
69. Inoue, K., et al., *Osteopenia and male-specific sudden cardiac death in mice lacking a zinc transporter gene, Znt5.* Human Molecular Genetics, 2002. **11**(15): p. 1775-1784.
70. Guo, Y. and Y. He, *Comprehensive analysis of the expression of SLC30A family genes and prognosis in human gastric cancer.* Scientific Reports, 2020. **10**(1): p. 18352.
71. Irwin, C.R., et al., *In-Fusion® Cloning with Vaccinia Virus DNA Polymerase*, in *Vaccinia Virus and Poxvirology: Methods and Protocols*, S.N. Isaacs, Editor. 2012, Humana Press: Totowa, NJ. p. 23-35.
72. Bird, L.E., et al., *Application of In-Fusion™ Cloning for the Parallel Construction of E. coli Expression Vectors*, in *DNA Cloning and Assembly Methods*, S. Valla and R. Lale, Editors. 2014, Humana Press: Totowa, NJ. p. 209-234.
73. TakaraBio. 10/11/2022]; In-Fusion Cloning overview]. Available from: https://www.takarabio.com/learning-centers/cloning/in-fusion-cloning-general-information/in-fusion-cloning-overview.
74. Stepanenko, A.A. and H.H. Heng, *Transient and stable vector transfection: Pitfalls, off-target effects, artifacts.* Mutat Res Rev Mutat Res, 2017. **773**: p. 91-103.
75. Bolognesi, B. and B. Lehner, *Reaching the limit.* eLife, 2018. **7**: p. e39804.
76. Gao, H.-L., et al., *Golgi apparatus localization of ZNT7 in the mouse cerebellum.* Histology and histopathology, 2009. **24**(5): p. 567-572.
77. Hoch, E., et al., *Histidine pairing at the metal transport site of mammalian ZnT transporters controls Zn2+ over Cd2+ selectivity.* Proc Natl Acad Sci U S A, 2012. **109**(19): p. 7202-7.
78. Baltaci, A.K. and K. Yuce, *Zinc Transporter Proteins.* Neurochemical Research, 2018. **43**(3): p. 517-530.
79. Alberts, B., et al., *Molecular Biology of the Cell, 4th edition*. 2002, New York: Garland Science.
80. Zimmermann, R., et al., *Protein translocation across the ER membrane.* Biochimica et Biophysica Acta (BBA) - Biomembranes, 2011. **1808**(3): p. 912-924.

APPENDIX 1: Solutions

Gel electrophoresis and gel extraction:

TAE buffer

40 mM Tris base

20 mM acetic acid

1 mM EDTA

Transformation:

LB medium

10 g BD BactoTM Tryptone

5 g BD BactoTM Yeast Extract

10 g NaCl

Adjust pH to 7.0

Add mqH_2O until 1 L

SDS-PAGE and Western Blotting:

RIPA buffer

1 mL RIPA
10x PMSF
10x PIC (protease inhibitor cocktail)

MES buffer

50 ml NuPAGE MES SDS Running Buffer (20x) (Invitrogen)
Adjust with mqH_2O until 1.0 L

Transfer buffer

50 mL NuPAGE™ Transfer buffer (20x) (Invitrogen)
100 mL Methanol (VWR chemicals)
Adjust with mqH_2O until 1.0 L

TBS (10x)

24 g Tris

88 g NaCl

900 mL mqH_2O

Adjust pH to 7.6 w/HCl

Add mqH_2O until 1.0 L

Block buffer

2.5 mL Odyssey Intercept™ blocking buffer (LI-COR)
2.5 mL TBS (1x)

TBS-T

1 L TBS (1x)

1 ml Tween® 20 (Sigma-Aldrich)

Protein purification:

Lysis buffer

50 mM Tris pH 7.6
500 mM NaCl
0.5 % Triton
1 mM DTT
1 mg/mL Lysozyme
3 tablets Protease Inhibitors
5 mM EDTA

Wash buffer with triton

50 mM Tris pH 7.6
500 mM NaCl
0.5 % Triton
1 mM DTT
5 mM EDTA

Wash buffer without triton

50 mM Tris pH 7.6
500 mM NaCl
1 mM DTT
5 mM EDTA

Elution buffer

500 mM NaCl
10 mM Reduced glutathione
50 mM Tris pH 8.0

Storage buffer

500 mM NaCl
50 mM Tris pH 8.0
5% Glycerol
1 mM DTT

GFP-tag IP:

Dilution buffer

50 mM Tris pH 7.5
150 mM NaCl
0.5 mM EDTA

APPENDIX 2: Primers

ZnT5 (SLC30A5)

Final primers ordered for amplification of ZnT5:

3522_SLC30A5_C1_FWD: GA CTC AGA TCT GGA Gct ATG GAG GAG AAA TAC GG

3523_SLC30A5_C1_RV_STOP: AGA TCC GGT GGA TCC CTA CAT GAT ATA GGT GCC ATC

3524_SLC30A5_N1_FWD: GAC TCA GAT CTC GAG ATG GAG GAG AAG TAC GG

3524_SLC30A5_N1_RV_NOSTOP: CGC ACC GGT GGA TCC cgC ATG ATA TAG GTG CCA TC

Sequence from pEGFPC1 plasmid

Sequence from pEGFPN1 plasmid

ZnT7 (SLC30A7)

Final primers ordered for amplification of ZnT77:

3433_SLC30A7_C1_FWD: GA CTC AGA TCT CGA Gct ATG TTG CCC CTG TCC ATC AA

3434_SLC30A7_C1_RV_STOP: AGA TCC GGT GGA TCC CTA CAT GGC TGC AAA GTC AAT C

3435_SLC30A7_N1_FWD: GAC TCA GAT CTC GAG ATG TTG CCC CTG TCC ATC AA

3436_SLC30A7_N1_RV_NOSTOP: CGC ACC GGT GGA TCC gcC ATG GCT GCA AAG TCA ATC TGT

Sequence from pEGFPC1 plasmid

Sequence from pEGFPN1 plasmid

Sequencing primers (for sequencing at EUROFINS)

448-EGFP_C	CATGGTCCTGCTGGAGTTCGTG
447-EGFP_N	CGTCGCCGTCCAGCTCGACCAG

220-CMV-for	cgcaaatgggcggtaggcgtg
1244-SV40t.REV	tgaaatttgtgatgctattgc

APPENDIX 3: PCR programs

PCR program 1:

Step	Temperature	Time
Initial Denaturation	98 °C	30 s
Denaturation	98 °C	8 s
Annealing*	52 °C 60 °C	15 s
Extension	72 °C	30 s
	Cycles: 35x	
Final Extension	72 °C	7 min
Hold	4 °C	∞

* = Represent different annealing temperatures used for the two different genes. For the amplification of ZnT5 an annealing temperature of 52°C was used whereas for the amplification of ZnT7 an annealing temperature of 60°C was used.

PCR program 2: Gradient PCR

Step	Temperature	Time
Initial Denaturation	98 °C	30 s
Denaturation	98 °C	8 s
Annealing*	49.7-52.8 °C 61.7-65.5 °C	15 s
Extension	72 °C	30 s
	Cycles: 35x	

Final Extension	72 °C	7 min
Hold	4 °C	∞

* = Represents different gradients of annealing temperatures used. This gradient ranges from 49.7-52.8 °C in one group (for the amplification of ZnT5) and 61.7-65.5 °C in the other group (for the amplification of ZnT7).

PCR program 3:

Step	Temperature	Time
Initial Denaturation	98 °C	30 s
Denaturation	98 °C	8 s
Annealing*	52.8 °C 65.5 °C	15 s
Extension	72 °C	30 s
	Cycles: 35x	
Final Extension	72 °C	7 min
Hold	4 °C	∞

* = Represents different annealing temperatures used. ZnT5 was amplified used an annealing temperature of 52.8 °C. ZnT7 was amplified using an annealing temperature of 65.5 °C.